ACES Asian Chemical Editorial Society

DOI: 10.1002/asia.201700469

CHEMISTRY AN ASIAN JOURNAL Full Paper

Vanadium | *Very Important Paper*

VIP

SPECIAL ISSUE

Interaction of $[V^{IV}O(acac)_2]$ with Human Serum Transferrin and Albumin

Isabel Correia,[a] Ielyzaveta Chorna,[a] Isabel Cavaco,[a, b] Somnath Roy,[a, c] Maxim L. Kuznetsov,[a] Nádia Ribeiro,[a] Gonçalo Justino,[a] Fernanda Marques,[a, d] Teresa Santos-Silva,[e] Marino F.A. Santos,[e] Hugo M. Santos,[e, f] José L. Capelo,[e, f] James Doutch,[g] and João Costa Pessoa*[a]

Abstract: $[VO(acac)_2]$ is a remarkable vanadium compound and has potential as a therapeutic drug. It is important to clarify how it is transported in blood, but the reports addressing its binding to serum proteins have been contradictory. We use several spectroscopic and mass spectrometric techniques (ESI and MALDI-TOF), small-angle X-ray scattering and size exclusion chromatography (SEC) to characterize solutions containing $[VO(acac)_2]$ and either human serum apotransferrin (apoHTF) or albumin (HSA). DFT and modeling protein calculations are carried out to disclose the type of binding to apoHTF. The measured circular dichroism spectra, SEC and MALDI-TOF data clearly prove that at least two VO–acac moieties may bind to apoHTF, most probably forming $[V^{IV}O(acac)(apoHTF)]$ complexes with residues of the HTF binding sites. No indication of binding of $[VO(acac)_2]$ to HSA is obtained. We conclude that $V^{IV}O$–acac species may be transported in blood by transferrin. At very low complex concentrations speciation calculations suggest that [(VO)(apoHTF)] species form.

1. Introduction

Bis(acetylacetonato)oxidovanadium(IV), or $[V^{IV}O(acac)_2$ (**1**), is one of the most remarkable vanadium compounds. In the solid state it consists of discrete molecules of $[V^{IV}O(acac)_2$ in which vanadium(IV) presents an almost square pyramidal geometry (Figure 1).[1] It forms quite stable $V^{IV}O$-complexes,[2,3] the reported stability constants in aqueous solution being log $\beta_1 = 8.73$ and log $\beta_2 = 16.27$, respectively.[4]

$[V^{IV}O(acac)_2]$ has found uses in multiple areas. Namely, it has been used as the vanadium precursor for the preparation of many vanadium complexes where one[5–7] or both[8,9] $acac^-$ ligands are replaced.[10] It has also been used directly as catalyst precursor in organic chemistry, for example, in aerobic oxidations,[10,11] epoxidations (e.g. of allylic alcohols, geraniol), sulfoxidations[12] in combination with *tert*-butylhydroperoxide or H_2O_2,[13,14] or immobilized in solid supports.[15]

$[V^{IV}O(acac)_2]$ exerts interesting biological effects; namely it exhibits insulin-enhancing properties, in that in can stimulate the phosphorylation of protein kinase B (PKB/Akt) and glycogen synthase kinase-3 (GSK3).[16] It has also been shown to inhibit tyrosine phosphatases (PTPases), such as PTP1B.[16] The effects of $[V^{IV}O(acac)_2]$, $[V^{IV}O(Et\text{-}acac)_2]$ and of a few other $V^{IV}O$-compounds on the glycemia of streptozotocin-induced diabet-

[a] *I. Correia, I. Chorna, I. Cavaco, S. Roy, M. L. Kuznetsov, N. Ribeiro, G. Justino, F. Marques, J. C. Pessoa*
Centro de Química Estrutural, Instituto Superior Técnico
Universidade de Lisboa
Av. Rovisco Pais, 1049-001, Lisboa (Portugal)
E-mail: joao.pessoa@ist.utl.pt

[b] *I. Cavaco*
Departamento de Química e Farmácia
Universidade do Algarve
Campus de Gambelas, 8005-139 Faro (Portugal)

[c] *S. Roy*
Department of Chemistry
Ananda Chandra College
Jalpaiguri, West Bengal (India)

[d] *F. Marques*
Centro de Ciências e Tecnologias Nucleares
Instituto Superior Técnico
Universidade de Lisboa
Estrada Nacional 10 (km 139.7), 2695-066 Bobadela LRS (Portugal)

[e] *T. Santos-Silva, M. F. Santos, H. M. Santos, J. L. Capelo*
UCIBIO, REQUIMTE, Departamento de Química, Faculdade de Ciências e Tecnologia
Universidade Nova de Lisboa
2829-516 Caparica (Portugal)

[f] *H. M. Santos, J. L. Capelo*
PROTEOMASS Scientific Society
Madan Park, Rua dos Inventores, 2825-152 Caparica (Portugal)

[g] *J. Doutch*
ISIS Pulsed Neutron and Muon Source, Science and Technology Facilities Council
Harwell Science and Innovation Campus, Didcot, OX11 0QX (UK)

Supporting information and the ORCID identification number(s) for the author(s) of this article can be found under https://doi.org/10.1002/asia.201700469.

This manuscript is part of a virtual issue on advances in vanadium chemistry. The complete issue can be found on the journal website www.chemasianj.org

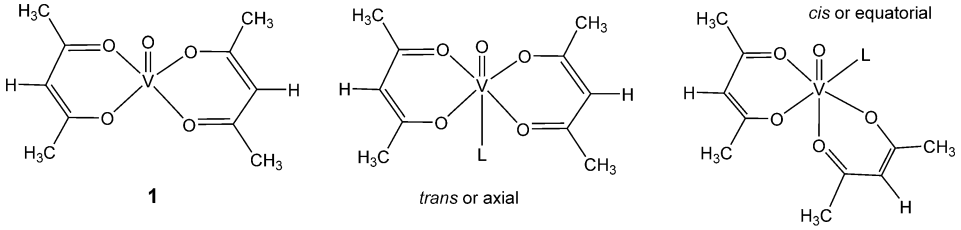

Figure 1. Structural formulae of $[V^{IV}O(acac)_2]$ (**1**) (left). In $[V^{IV}O(acac)_2(L)]$ complexes, the donor atom of ligand L may bind *trans* or *cis* to the O-oxido. If the binding is *trans*, also often called the axial position, no particular rearrangement of the two $acac^-$ ligands is required; if the binding is *cis*, also often called the equatorial position, one of the $acac^-$ ligands will then have one of its O-atoms bound *trans* to the O-oxido ligand (as in $[V^{IV}O(acac)_2(Phpy)]$, Figure 2).

ic rats (STZ-rats) were examined.[17,18] $[V^{IV}O(acac)_2]$ was also reported to have antiproliferative effects[2,19–21] and to have potential as both antidiabetic and antipancreatic cancer agent to prevent or treat patients suffering from both diseases.[19]

Another property of $[V^{IV}O(acac)_2]$ is its remarkable activity in degrading plasmid DNA in the absence of any activating agents, air and photoirradiation.[20,21] The nature of the pH buffer was found to be determinant in the nuclease activity, and in phosphate-buffered medium single-strand cleavage is clear for concentrations of **1** as low as 1.2 μM (corresponding to a ri = 0.08), and in the presence of activators it is much more extensive.[20,21] The mechanism is oxidative and mainly associated with the formation of reactive oxygen species (ROS).[21] Hydrolytic cleavage of the phosphodiester bond is also promoted by **1**, but at much slower rate, not competing with the oxidative mechanism.[20] These properties may have important implications in the interpretation of the biological activity of $[V^{IV}O(acac)_2]$.

$[V^{IV}O(acac)_2]$ thus exhibits insulin-enhancing properties and several other relevant biological effects.[2,16,22,23,24] Since human serum albumin (HSA) serves as a drug transport carrier and human serum transferrin (HTF) is an important metal ion blood carrier, the understanding of the interactions that may be established between $[V^{IV}O(acac)_2]$ and these plasma proteins is of major importance to understand its pharmacokinetics and pharmacodynamics. Additionally, most proposals explaining the insulin-enhancing properties of vanadium compounds involve formation of protein-vanadium complexes, namely in blood,[21] thus, the understanding of the speciation of $[V^{IV}O(acac)_2]$ in blood and how this might be important in the uptake of vanadium by cells, are relevant issues.

Regarding the transport of vanadium compounds in blood in vivo, most studies agree that these are predominantly transported bound to serum proteins, particularly HTF.[24–32] More recently the uptake of V-species by red blood cells (RBCs) and its possible role was highlighted,[33–35] but at the low total vanadium concentrations expected in vivo in the blood following oral administration of V antidiabetics, most probably significantly less than ca. 20 μM even upon oral treatment with a VC,[30,36] HTF appears to be the main vanadium transporter and RBCs possibly play some role in the pharmacokinetics of these compounds and in providing a reducing effect, eventually allowing the formation of V^{III}, which may strongly bind to HTF.[37]

The binding of $[V^{IV}O(acac)_2]$ to albumin was studied by EPR and ENDOR spectroscopies,[38] and Mustafi et al.[39] used isothermal titration calorimetry (ITC) and spectrofluorometry to determine the binding constant of $[V^{IV}O(acac)_2]$ to bovine serum albumin (BSA). It was reported that glucose uptake by 3T3-L1 adipocytes was significantly higher when using $[V^{IV}O(acac)_2]$ in the presence of HSA (when the albumin: $[V^{IV}O(acac)_2]$ ratio $\geq$ 1.0).[2,38] These authors also stated that serum albumin enhanced the insulin-like activity of all studied V-complexes, including **1**, more than human serum transferrin,[40] and that the characteristics described are related to the high stability and capacity of $[V^{IV}O(acac)_2]$ to remain intact upon binding to HSA. Moreover, the specificity of **1** for highly glycolytic cells, its low toxicity[25] and its *anti*-tumorigenic properties[23,24,41,42] contribute to make **1** a potentially useful contrast agent for early tumor detection, and possibly also for treatment. The advantage of $[V^{IV}O(acac)_2]$ for this purpose would result from its binding to serum albumin increasing its serum half-life and allowing its transport and delivery to its targeted tumor site.[39]

Garribba and co-workers[27,29,43–45] studied extensively the binding of $V^{IV}O$-complexes to blood components, mainly by using EPR spectroscopy. Namely, the anisotropic EPR spectra of solutions containing $V^{IV}O^{2+}$-HTF, $V^{IV}O^{2+}$-acac, $V^{IV}O^{2+}$-apoHTF-acac and $V^{IV}O^{2+}$-holoHTF-acac, in the presence and absence of other blood serum components, were recorded at pH 7.4. Globally the authors report that two different species could be distinguished, one in higher concentration, identified as $(V^{IV}O)_2$apoHTF, and the 2nd one as $[V^{IV}O(acac)_2]$, and no $V^{IV}O$-acac-apoHTF species were identified. These authors further stated that the EPR spectroscopic data suggest that no mixed complexes are formed, this being in agreement with acetylacetonate not acting as a synergistic anion.[29,45] In similar studies with HSA, the authors report that only $[V^{IV}O(acac)_2]$ is detected, and that the EPR spectra of solutions containing $[V^{IV}O(acac)_2]$ and 1-methylimidazole are practically indistinguishable from those of the binary system $V^{IV}O^{2+}$-acac,[29] no $V^{IV}O$-acac-HSA species being identified.[29,44] Similar conclusions were made from the measurement of the anisotropic EPR spectra of solutions containing $[V^{IV}O(acac)_2]$ and holoHTF: no $[V^{IV}O(acac)_2$(holoHTF)] species were detected,[45] and again it was considered that $[V^{IV}O(acac)_2]$ has a square-pyramidal coordination geometry and has no tendency to form complexes of the type *cis*-$[V^{IV}O(carrier)_2$(protein)], this being allegedly corro-

borated by the conclusion that no ternary species are formed by $V^{IV}O^{2+}$, acetylacetonate and 1-methylmidazole. Similar conclusions were made by the same group in studies with Immunoglobulin G.[43]

Notwithstanding, contradicting the initial statements of Selbin,[46] $[V^{IV}O(acac)_2]$ is a weak Lewis acid, and for example, upon dissolution in organic solvents or in solutions containing potential ligands, the vanadium may coordinate a donor ligand in the vacant site, forming complexes expressed as $[VO(acac)_2(L)]$, sometimes designated as adducts, with for example, amide, amine, sulfoxide and pyridine solvents/ligands,[3] and this process [Eq. (1)] has been studied by several methods.[3,47,48–54]

$$[V^{IV}O(acac)_2] + L \rightleftharpoons [V^{IV}O(acac)_2(L)] \quad (1)$$

In earlier work, solvent effects were explained by coordination to the vacant axial position, but this was later questioned in several publications[3] and the available literature is not always in agreement. In fact, in solution, while some authors state that $[V^{IV}O(acac)_2]$ bind solvents in *trans* position,[49,50] several studies also showed that some solvents bind to the V^{IV} equatorially, and other publications report either *cis*- or *trans*-binding depending on the ligand added.[51–53] With some solvents, the interaction (e.g. hydrogen bonding) with the O-oxido ligand has also been proposed.[55–58] For example, IR studies with pyridine derivatives demonstrated the existence of adducts with the sixth ligand bound *cis* rather than *trans* to the oxido O-atom (Figure 1),[52,54] and ENDOR studies showed that while for example, methanol binds to the vacant axial 6th position, it was shown that either *cis* or *trans* isomers are formed with some substituted pyridines.[51] In fact, although this may result from solid state effects, a single crystal X-ray diffraction (XRD) study of the 4-phenylpyridine (Phpy) adduct **3** confirmed the possibility of *cis* binding of substituted pyridines (Figure 2).[59] On the other hand, the structure determined by single crystal XRD of $[V^{IV}O(acac)_2$(4-methylpyridine)$]$ consists of discrete molecules with 4-methylpyridine in the *trans* position and short $V{=}O$ (1.557 Å) and long V-N (2.447 Å) bond lengths.[60] In the adduct formed with dioxan, $[V^{IV}O(acac)_2$(dioxan)$]$,[61] the dioxan bridges two $[V^{IV}O(acac)_2]$ molecules axially (*trans*) to the V centers; in $[V^{IV}O(acac)_2$(2-pyridone)$]$ the 2-pyridone is bound axially,[62] as pyrazole (Pz) in $[V^{IV}O(acac)_2(Hpz)]$ (**2**).[63]

Overall, taking into account the literature data, the interaction of ligands (solvent or a dissolved molecule) with $[V^{IV}O(acac)_2]$ may involve:[3] (i) coordination in a sixth position *trans* to the oxido O-atom, (ii) coordination in a sixth position *cis* to the oxido O-atom, and (iii) hydrogen bonding to the O-oxido or atoms of the ligand (e.g. with chloroform[51,56]).

HTF has 8 tryptophan residues (3 in the *N*-lobe, 5 in the C-lobe) and 25 tyrosines (14 in the *N*-lobe, 12 in the C-lobe).[64] The two iron binding sites are located near the junction of two domains formed by Cys-117 to Cys-194 bond in the N-terminus. Potential amino acid residues that may act as ligands for V^{IV} in the iron binding sites are Tyr188, Tyr95, His249 and Asp63 (*N*-lobe) and Tyr426, Tyr517, His585 and Asp392 (C-lobe). Side groups of other residues of HTF may bind V^{IV}, namely imidazole donors from histidines, and His-14, His-289, His-349, His-350, His-473, His-606 and His-642 have been considered as good candidates.[45] The structure of human serum albumin consists of a single polypeptide chain with 585 amino acid residues, with a 3-dimensional structure normally described in terms of 3 homologous chains (I, II and III), each of them formed by two subdomains (A and B). HSA has one tryptophan residue (Trp214 located in subdomain II-A) and 18 tyrosine residues.

As described above, there are many reports on in vitro and in vivo experiments proving several relevant biological effects of $[V^{IV}O(acac)_2]$. It has been repeatedly emphasized[2,4,45,65] that $[V^{IV}O(acac)_2]$ is a stable entity. However, there are also many studies confirming the formation of mixed-ligand complexes $[V^{IV}O(acac)_2(L)]$ or $[V^{IV}O(acac)(L1)(L2)(L3)]$. Therefore, the formation of such complexes where L1, L2 and L3 could be donor atoms from HTF (or HSA) appears plausible. The binding to HTF could involve some of the donor atoms of the Fe-binding site, or donor atoms of side groups of other amino acid residues. This reasoning and the contradictory reports of the groups of Garribba and Makinen, regarding the binding of $[V^{IV}O(acac)_2]$ to HSA (and apoHTF), and the conclusion of Garribba and co-workers that *cis*-$[V^{IV}O(acac)_2$(protein)$]$ or $[V^{IV}O(acac)$(protein)$]$ do not form with serum proteins, mainly based on EPR spectroscopic measurements, when there are many other papers confirming the formation of $[V^{IV}O(acac)_2(L)]$ and $[V^{IV}O(acac)(L)]$ compounds, made us study the systems V^{IV}O-acac-HTF and V^{IV}O-acac-HSA using several distinct experimental techniques to clearly prove if V^{IV}O-acac species can bind these proteins or not.

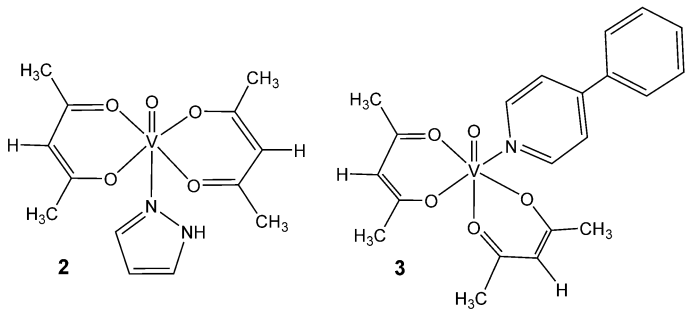

2. Results and Discussion

2.1. $[V^{IV}O(acac)_2]$ in aqueous solution.

2.1.1. UV/Vis absorption studies.

In aqueous solutions of $[V^{IV}O(acac)_2]$ Crans and co-workers[17,65] reported the observation of three species by EPR spectroscopic measurements at room temperature whose concentrations were time, pH, temperature and salt dependent. The three com-

plexes were assigned as the *trans*-[$V^{IV}O(acac)_2(H_2O)$], *cis*-[$V^{IV}O(acac)_2(H_2O)$] and a $V^{IV}O$-hydrolysis product containing one $acac^-$ ligand. No evidence for V^V was found in fresh solutions of [$V^{IV}O(acac)_2$], but slow oxidation occurs.[17] The speciation diagram depicted in Figure 3 shows that in the system $V^{IV}O^{2+}$ + acac around the physiological pH $V^{IV}O$ is mostly present as the neutral complex [$V^{IV}O(acac)_2$], the hydrolysis degree being low. At pH ≈ 3.3 [$V^{IV}O(acac)^+$] species predominate, while for pH < 2.0 [$V^{IV}O(H_2O)_5^{2+}$] is the predominant $V^{IV}O$-complex.

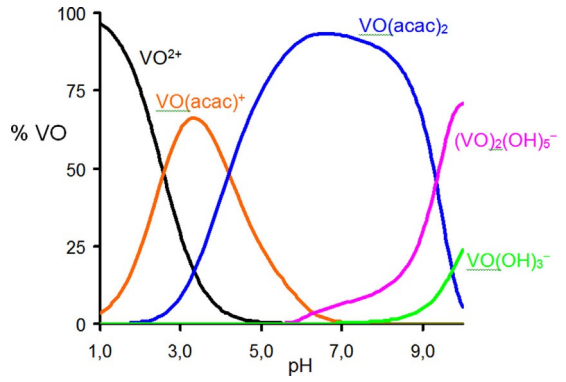

Figure 3. Speciation diagram calculated for total $V^{IV}O$ and acetylacetone concentrations of 2 and 4 mM, respectively, considering the formation constants log $\beta_1 = 8.73$ and log $\beta_2 = 16.27$, reported in [4] and the $V^{IV}O$-hydrolytic constants: [$VO(OH)^+$], [$(VO)_2(OH)_2^{2+}$], [$(VO)_2(OH)_5^-$] and [$VO(OH)_3^-$] in refs. [3, 25].

Mustafi et al and Makinen et al.[2, 38, 58] provided a distinct speciation diagram where [$V^{IV}O(acac)_2$] is considered stable in aqueous solutions of pH 2. However, this contradicts other observations,[4, 17] considered compatible with the formation of [$V^{IV}O(H_2O)_5^{2+}$]→[$V^{IV}O(acac)^+$]→[$V^{IV}O(acac)_2$] as the pH is increased. In the SI section we discuss why we consider Figure 3 to correspond to the correct speciation, also demonstrating that [$V^{IV}O(acac)_2$] is not stable in aqueous solutions of pH 2.

As mentioned above, there are several studies in the literature reporting the coordinative binding of amines and of other monodentate ligands to [$V^{IV}O(acac)_2$] in solution, namely including the determination of binding constants K [Eqs. (1) and (2)].[47, 48]

$$K = \frac{[VO(acac)_2(L)]}{[VO(acac)_2][L]} \quad (2)$$

Most of these studies were done by electronic absorption measurements in organic solvents (e.g. benzene, nitrobenzene, dichloromethane); for example, for pyridine the values determined in CH_2Cl_2 and benzene were 867 ± 53[48] and 56 ± 5,[47] respectively. The value of K obviously also depends on the amine considered; for example, for piperidine and pyrrolidine, the values determined in benzene were 1400 ± 400 and 2900 ± 1000,[47] respectively. In aqueous media the K values will certainly differ from these, and the degree of formation of the adducts [$V^{IV}O(acac)_2(L)$] will also depend on the pH of the solution and pK_a of the amine.

We measured the spectra of aqueous solutions containing [$V^{IV}O(acac)_2$] and several potentially monodentate ligands (see experimental and SI sections for details): imidazole, 2-Me-imidazole, benzimidazole, pyrazole, 4-*t*-buthylphenol at pH 7.0 ± 0.2. Considering the speciation diagram of the $V^{IV}O$-acac system with $C_{VO} = 2$ mM and $C_{acac} = 4$ mM (Figure 3), in the pH range ca. 6.2–7.2 the amount of [$V^{IV}O(acac)_2$] is maximized, while maintaining its hydrolysis at a reasonable low level (less than ca. 5% of total vanadium). Figure 4 depicts data for imidazole and pyrazole. The absorption spectra of these solutions were measured in the range 380–900 nm, each measurement starting always after the same period of time upon adding the required amount of the [$V^{IV}O(acac)_2$] solution (in MeOH) to the aqueous solution containing the buffered solution of the ligand L. The additions of imidazole, 2-Me-imidazole, or pyrazole to the [$V^{IV}O(acac)_2$] solutions all yielded an increase in the absorbance values in the range 380–900 nm. This effect is clearly observable at a L:[$V^{IV}O(acac)_2$] ratio of 1:1, but larger amounts of ligand present in the final solution almost did not cause further increase; because no significant shift of the absorption maxima is seen in these visible absorption spectra probably the interaction is weak.

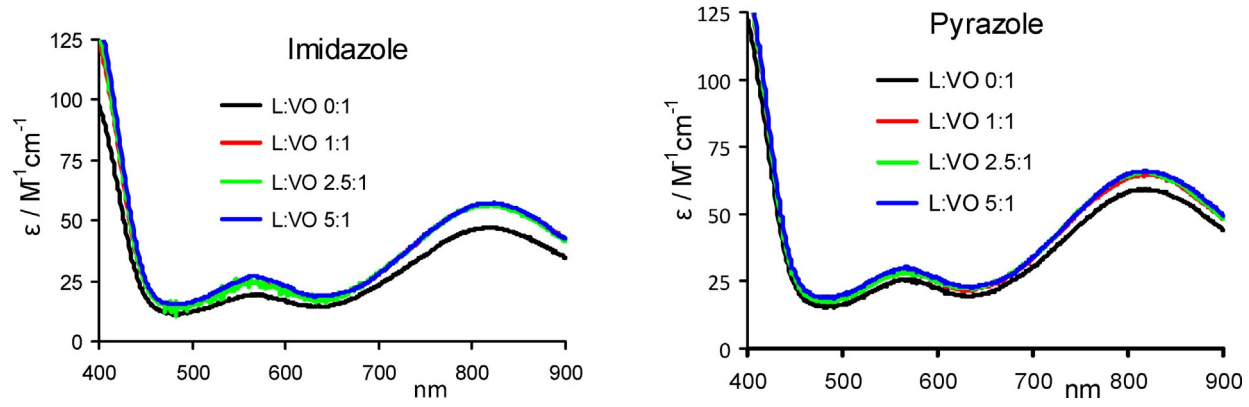

Figure 4. Absorption spectra of solutions of [$V^{IV}O(acac)_2$] added to solutions of (A) imidazole (Im), and (B) pyrazole (Pz) containing a 40 mM carbonate buffer. The maximum amount of methanol of the samples was ca. 3%. The spectra recorded correspond to independent samples with a concentration of [$V^{IV}O(acac)_2$] of 2.0 mM and pH 7.0 ± 0.2. The L:[$V^{IV}O(acac)_2$] ratios are indicated.

It is clear that, in the presence of imidazole (or 2-Me-imidazole or pyrazole), a significant global increase in the ε values in the 380–900 nm range takes place, which can only be explained by the binding of the N(3) atom of imidazole (or *N*-atoms of 2-Me-imidazole or pyrazole) to $[V^{IV}O(acac)_2]$. It may be observed that for Im:$[V^{IV}O(acac)_2]$ ratios of 1:2 or 1:4 the spectra do not differ much from the one recorded at a 1:1 ratio, this meaning that at this ratio most of the imidazole was already bound to $[V^{IV}O(acac)_2]$. The possibility of non-coordinating interactions explaining the increase in absorption values cannot be ruled out. However, the change in the spectra observed is similar to those observed in the monodentate binding of O-carboxylate of several hydroxycarboxylic acids[66] and amino acids,[67–73] where the monodentate coordinative binding was demonstrated by several spectroscopic methods and pH-potentiometric titrations.

To further prove the possibility of monodentate binding of these monodentate ligands to $[V^{IV}O(acac)_2]$, rather similar experiments were carried out with L-lactic acid at pH ≈ 6.0; these are described in the SI section (SI-8.4). Figure SI-8.4-1 depicts absorption spectra of some of these solutions and Figure SI-8.42 the CD spectra. There are some subtle changes in the absorption spectra of the solutions at $\lambda_{max} \approx 560$ and 820 nm akin to those observed in the similar experiments described above (e.g. Figure 4). Importantly, weak but clearly measurable CD spectra were recorded with the same samples which can only be explained by the coordinative monodentate binding of the O-carboxylate to $[V^{IV}O(acac)_2]$. If this corresponded to bidentate binding the absorption spectra would certainly have distinct λ_{max} from those of $[V^{IV}O(acac)_2]$, and that is not the case. Establishment of hydrogen bonding of the O-hydroxyl of lactate to the O-oxido or to O-acac atoms cannot be ruled out.

The additions of benzimidazole and of 4-*tert*-butylphenol were examples where this effect of absorption increase did not depict a clear trend (see SI section). In the case of benzimidazole possibly because of steric hindrance; in the case of 4-*tert*-butylphenol probably also because of its relatively high pK_a value (10.2), thus at pH 7.0 the phenolic OH remains protonated and its propensity to bind $[V^{IV}O(acac)_2]$ is low.

2.1.2. Mass spectrometric studies.

To further confirm the formation of $[V^{IV}O(acac)_2(L)]$ species in aqueous media, solutions of the same potentially monodentate ligands: imidazole, methylimidazole, benzimidazole, pyrazole and phenol (this instead of 4-*tert*-butylphenol) were prepared in 10 mM NH_4CH_3COO aqueous solution (previously set to pH 6.5). Accurately measured volumes of each of these solutions and of the NH_4CH_3COO aqueous solution were added to six distinct vials, and accurately measured volumes of $[V^{IV}O(acac)_2]$ in methanol (80 mM) was added to each of the six vials. Final solutions were 1.1 mM in $[V^{IV}O(acac)_2]$ and 2% v/v MeOH, and the molar ratios ligand:$V^{IV}O$ was 7:1 in all samples; pH values ranged from 6.58 to 7.15.

For each of the six solutions, ESI-MS (+/-) was carried out ca. 5–10 minutes after the addition of $[V^{IV}O(acac)_2]$; samples of these solutions were also taken for EPR spectroscopic measurements and immediately frozen in liquid N_2 (see below). The ESI-MS of the solution containing only $[V^{IV}O(acac)_2]$ differed significantly from those of $[V^{IV}O(acac)_2]$ and monodentate ligands. The results of these experiments are described in the SI section and the data is summarized in Table 1. Globally the mass spectrometric data confirm the formation of $[V^{IV}O(acac)_2(L)]$ species in aqueous media for L = imidazole, methylimidazole, benzimidazole and pyrazole. Only in the case of L = phenol no assignments could be made confirming the formation of $[V^{IV}O(acac)_2(phenolato)]$ in the conditions used.

2.1.3. EPR spectroscopy studies.

With the solutions prepared for the MS experiments mentioned in the previous section, samples were collected for EPR spectroscopic measurements. The results are described in the SI-section. All measured EPR spectra for aqueous solutions at pH ca. 6.6–7.1 of $[V^{IV}O(acac)_2]$ and of $[V^{IV}O(acac)_2]$ + L (L = imidazole, methylimidazole, benzimidazole, pyrazole and phenol) and almost superimposable, thus it is plausible that the interaction of these ligands with $[V^{IV}O(acac)_2]$ is axial. Figure SI-8.3-

Table 1. Summary of assignments in ESI-MS experiments with solutions of $[V^{IV}O(acac)_2]$ upon addition to solutions of several potential monodentate ligands. [a]

System and tentative assignment	Mass observed	System and tentative assignment	Mass observed
$[V^{IV}O(acac)_2]$		$[V^{IV}O(acac)_2]$ + Imidazole	
$[V^{IV}O(acac)_2\text{-H}]^-$	(−) 264.04	$[V^{IV}O(acac)_2(Im)\text{-H}]^-$ (?)	(−) 331.58
$[V^{IV}O(acac)_2 + H]^+$	(+) 266.08	$[V^{IV}O(acac)_2(Im) + H]^+$	(+) 333.65
$[V^{IV}O(acac)_2 + MeOH + H]^+$	(+) 297.9	$[V^{IV}O(acac)(Im)_2]^+$	(+) 301.9
$[V^{IV}O(acac)_2 + H_2O + H]^+$	(+) 283.9		
$V^{IV}O(acac)_2{}^{\cdot} + V^{IV}O(acac)^+$ (?)	(+) 430.96		
$[V^{IV}O(acac)_2]$ + Me-Imidazole		$[V^{IV}O(acac)_2]$ + pyrazole	
$[V^{IV}O(acac)_2(MeIm)\text{-H}]^-$	(−) 381.49	–	–
$[V^{IV}O(acac)_2(MeIm) + H_2O + H]^+$	(−) 317.91	$[V^{IV}O(acac)_2(Pz) + H_2O + H]^+$	(+) 351.91
$[V^{IV}O(acac)(MeIm)_2 + H]^+$	(+) 384.3	$[V^{IV}O(acac)(Pz)]^+$	(+) 231.14
$[V^{IV}O(acac)_2(MeIm) + H_2O + Na^+]^+$	(+) 401.91	$[V^{IV}O(acac) + 2(Pz)]^+$	(+)302.00
$[V^{IV}O(acac)_2]$ + Benzimidazole		$[V^{IV}O(acac)_2]$ + phenol	
$[V^{IV}O(acac)_2(Bz)]^-$	(−) 381.49	No assignment	
$[V^{IV}O(acac)(Bz) + (OH^-)_2]^-$	(−) 317.91		
$[V^{IV}O(acac)_2(Bz) + H]^+$	(+) 384.3		
$[V^{IV}O(acac)_2(Bz) + H_2O + H]^+$	(+) 401.91		

[a] Although during the ESI process free ligands may bind non-specifically to $[V^{IV}O(acac)_2]$, resulting in false positives,[74,75] we explain our our data considering coordinative binding. Non-coordinative binding is much more probable with solvent or buffer molecules, present in much higher amounts.

25 depicts the low field range of these spectra. Thus, although the visible absorption and mass spectrometric measurements indicate the formation of $[V^{IV}O(acac)_2(L)]$ complexes in aqueous solution, the EPR spectra of all systems measured are almost equal and superimposable with the EPR spectrum of $[V^{IV}O(acac)_2]$.

2.2. Interaction of $[V^{IV}O(acac)_2]$ with human serum transferrin

2.2.1. Circular dichroism

In the visible range, because the protein does not absorb, only charge transfer or $V^{IV}O$-d-d electronic transitions are observed. Thus, clearly measurable $\Delta\varepsilon$ values can only be recorded in the visible range of the circular dichroism (CD) spectra when there is coordination of donor atoms of the protein to vanadium(IV); otherwise no induced CD-bands due to charge transfer or d-d transitions can be measured.[31,67,76,77]

The type of spectrum obtained for $V^{IV}O$-compounds in the visible range depends on the particular binding and environment of the chiral donors around the $V^{IV}O$ center. If more than one chiral $V^{IV}O$-complex forms in solution, the measured CD spectrum is the weighted sum of the CD spectra of all $V^{IV}O$-complexes formed in the system being studied, each corresponding to a set of distinct $\Delta\varepsilon(\lambda)$ values (see SI-section). Figure 5 includes CD spectra in the 400–1000 nm range of solutions containing apoHTF and $V^{IV}OSO_4$ (blue lines). It is known and accepted[26,27,29,31,34,64,68,78] that in such solutions the $V^{IV}O^{2+}$ is bound by donor atoms of residues of the iron binding site of HTF, forming either 1:1 or 2:1 ($V^{IV}O$:apoHTF ratio) complexes.

The fact that non-zero $\Delta\varepsilon$ values are measured in the visible range for solutions containing $[V^{IV}O(acac)_2]$ and apoHTF (Figure 5) and that the pattern of CD spectra obtained differs from those of solutions containing $V^{IV}OSO_4$ and apoHTF (containing $(V^{IV}O)_n$HTF complexes), means that:

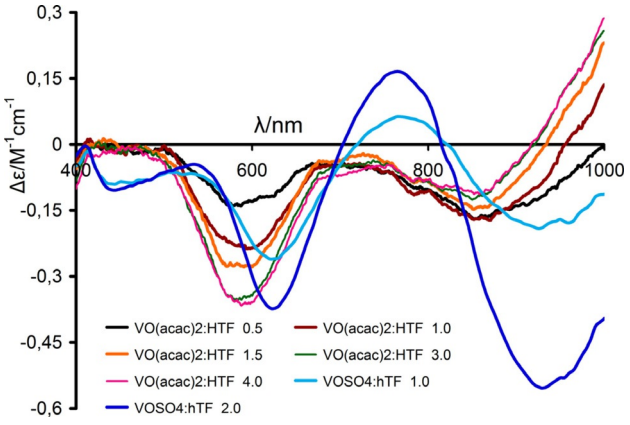

Figure 5. Circular dichroism spectra in the visible range of solutions containing apoHTF (≈600 μM) and $[V^{IV}O(acac)_2]$, and of $V^{IV}OSO_4$ and apoHTF (≈750 μM) at pH 7.4, with the indicated V^{IV}:apoHTF molar ratios. The baseline in this Figure corresponds to the CD spectrum of the solution of apoHTF. A quartz cell with optical path of 2.0 cm was used.

(i) significant amounts of $V^{IV}O$-acac species bind to HTF and (ii) there is no extensive hydrolysis of the $V^{IV}O$-acac species leading to the formation of $(V^{IV}O)_n$HTF complexes.

It is also noteworthy that the order of magnitude of the measured $\Delta\varepsilon$ values for the system $[V^{IV}O(acac)_2]$ and apoHTF is the same as those measured for solutions containing $(V^{IV}O)_n$HTF complexes. From the CD spectra shown in Figure 5 it cannot be concluded with certainty what type of $V^{IV}O$-acac-HTF complexes are formed, but the relatively high $\Delta\varepsilon$ values measured suggests that a significant fraction of these complexes correspond to $[V^{IV}O(acac)(HTF)]$ species, where the $V^{IV}O$:acac molar ratio is 1:1, and the V^{IV} is bound to more than one chiral residue of apoHTF,[26] as otherwise the $\Delta\varepsilon$ values would be significantly lower, as was the case of those measured in solutions containing $[V^{IV}O(picolinato)_2]$ and lysozyme,[79] or in solutions containing $V^{IV}O^{2+}$ and amino acids with monodentate coordination of the α-COO^- moiety to V^{IV}.[67–72]

At least two distinct types of CD spectra may be distinguished in Figure 5, this also corresponding to at least two distinct $V^{IV}O$-acac complexes. In fact, in the spectrum of the solution with the $[V^{IV}O(acac)_2]$:apoHTF molar ratio of 1:0.5 (black line) the $\Delta\varepsilon$ values are <0 in the range 700–1000 nm (band I), corresponding to transitions $d_{xy}\rightarrow d_{xz},d_{yz}$ (both d_{xz} and d_{yz} have similar energy)[3] while for higher molar ratios two distinct bands (corresponding to $d_{xy}\rightarrow d_{xz}$ and $d_{xy}\rightarrow d_{yz}$, often designated by bands IA and IB) are clearly observed, the $\Delta\varepsilon$ values progressively increasing and becoming >0 for $\lambda > \approx 930$ nm as the $[V^{IV}O(acac)_2]$:apoHTF molar ratio increases. The two distinct patterns of the CD spectra measured imply that two different types of chiral $V^{IV}O$-acac-apoHTF species form as $[V^{IV}O(acac)_2]$ is added. It is also noteworthy that the addition of one more mole equivalent of $[V^{IV}O(acac)_2]$ to the solution with $[V^{IV}O(acac)_2]$:apoHTF molar ratio of 3 does not produce significant changes in the CD spectra measured. Thus, if more than two $V^{IV}O$-acac species bind to apoHTF, this is not clearly visible in the CD spectra measured.

2.2.2. Small-angle X-ray scattering (SAXS).

Data from native apo-transferrin were evaluated for concentration dependence using Primus,[80] and extrapolated to zero concentration. Using this method, a radius of gyration of 33.2 Å was derived from the experimental data, with approximate molecular weight of 74 kDa, and Porod volume 137 000 $Å^3$. This is in agreement with the known molecular weight of ≈79 kDa. The Kratky plot indicates a globular, multi-domain protein, as expected from the published PDB structures. The P(r) function derived from the data indicates D_{max} (the maximum atomic distance vector in the system) to be 112 Å as shown in Figure SI-9-1. Shape reconstruction using the data pipeline described in the SI section was carried out, with the filtered and refined structures shown in Figure SI-9-2. The data indicates interesting differences between the solution state structure and that derived from X-ray crystallography. Using the PDB model 2HAV,[81] a theoretical R_g (radius of gyration) of 31 Å was obtained using the CRYSOL package.[82] The

theoretical fit, shown in Figure SI-9-3, is satisfactory, suggesting that, despite the described R_g difference, the overall envelope shape of the solution state and crystallographic structure is similar.

A similar methodology was followed for the apoHTF-[$V^{IV}O(acac)_2$] sample. Comparing the results obtained from both samples, the sample containing apoHTF and [$V^{IV}O(acac)_2$] showed immediate, detectable differences on the SAXS length scales (Figure SI-9-4). In particular, the incubated sample was shown to possess significantly smaller radius of gyration at 30.8 Å, and smaller derived molecular weight, at 66 kDa. Moreover, even if the indicated globular structure is conserved, the normalized Kratky plot appears to indicate significant differences in domain structure from the native apoHTF. Not surprisingly, there is also a significant difference in the P(r) function between the native and the incubated sample (Figure 6) with

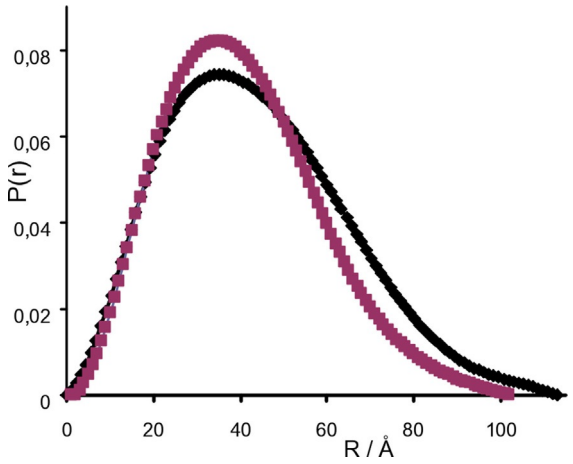

Figure 6. Superposition of pair distance distribution function for both analyzed samples—native apoHTF (black) and apoHTF-[$V^{IV}O(acac)_2$] (reddish)—highlighting their disparity.

the concomitant discrepancy in D_{max} values (112 Å and 104 Å, respectively). A shape reconstruction is shown in Figure SI-9-6. Therefore, the analysis of the SAXS data strongly suggests a clear modification on the conformation of apoHTF upon [$V^{IV}O(acac)_2$] binding, suggesting the existence of relatively strong protein-complex interactions.

2.2.3. Maldi-TOF Mass spectrometric data.

As described in the experimental section the samples for MALDI-TOF MS were prepared with apoHTF:[$V^{IV}O(acac)_2$] molar ratios of 1:0, 1:1, 1:2, 1:3 and 1:5 by mixing different volumes of the stock solutions with a NH_4HCO_3 buffer (pH 7.4, 25 mM). The results hereby reported were obtained with samples prepared by the Dried Droplet procedure, and each final spectrum was the accumulated result of at least 1000 laser shots that were obtained from 10 different manually selected regions of the same sample, over the range 14000–160000 Da.

In a set of experiments, the average mass obtained for apoHTF was 79247(±20), while the average mass obtained with samples containing 1:3 apoHTF:[$V^{IV}O(acac)_2$] molar ratios was 79581(±20). Thus, the difference in masses is significant (≈334). We assign this difference to the binding of two [$V^{IV}O(acac)^+$] moieties to apoHTF, which corresponds to ≈332 Da. Figure 7 depicts two representative Maldi-TOF mass spectra.

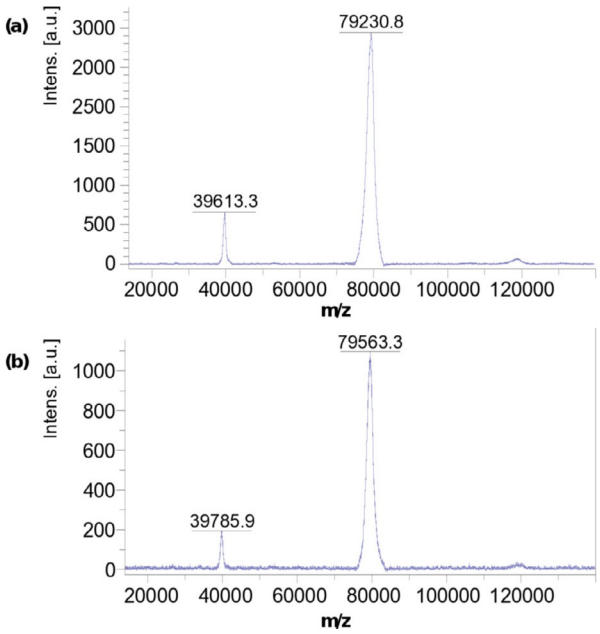

Figure 7. MALDI-TOF mass spectra obtained for samples of (a) apoHTF and (b) apoHTF + [$V^{IV}O(acac)_2$] (with 3:1 [$V^{IV}O(acac)_2$]:apoHTF molar ratios).

In a distinct set of experiments the [$V^{IV}O(acac)_2$]:apoHTF molar ratios were increased and the differences in masses were 201 (for 1:1), 346 (for 2:1) and 346 (for 3:1), this agreeing with the binding of one [$V^{IV}O(acac)^+$] moiety to apoHTF for the 1:1 molar ratio, and two for the 2:1 and 3:1 molar ratios. Interestingly, in similar MALDI-TOF experiments carried out with 5:1 [$V^{IV}O(acac)_2$]:apoHTF molar ratios the obtained average difference in mass between the samples of apoHTF and [$V^{IV}O(acac)_2$]:apoHTF was 653(±60, considering the several spectra obtained for different samples of these solutions). This is consistent with the binding to apoHTF of for example, two [$V^{IV}O(acac)(H_2O)^+$] moieties + one [$V^{IV}O(acac)_2$] (total mass = 633).

By doing experiments (described in the experimental section) doing laser shots in separate but very close spots, one containing the apoHTF, the other containing the solution of [$V^{IV}O(acac)_2$], where the *m/z* peaks obtained were equal to those of apoHTF alone, the existence of false positives can be ruled out (or at least the probability of their existence considered extremely low). We cannot totally rule out the possibility of non-covalent interactions explaining the increase in mass. However, it should be highlighted that the peak shapes (of *m/z* = 1 and 2) are both similar and sharp. If several different protein-complex interactions were established (as for non-covalent interactions), this would lead to broadening of the peaks.[83]

2.2.4. Use of size exclusion columns.

To further confirm the binding of $[V^{IV}O(acac)_2]$ to transferrin, solutions containing apoHTF (ca. 140 μM) and different amounts of $[V^{IV}O(acac)_2]$ were prepared, with molar ratios ranging from 1 to 8, and eluted with a tris buffer solution through desalting columns (PD-10 size exclusion columns, see experimental and SI sections). When using these columns the fractions first eluted contain apoHTF (and species bound to it), while the small molecules not bound to the macromolecule are retained inside the pores of the packing of the column, and are only eluted after significantly larger volumes of buffer pass through it. The eluate of the first eluted fractions were analyzed by inductively coupled plasma—atomic absorption spectroscopy (ICP-AES). The dilution effect from the elution (≈67%) was determined taking into account the absorbance of an apoHTF solution before and after eluting it, in experiments with no addition of $[V^{IV}O(acac)_2]$. Results of the ICP-AES analysis are included in Table 2. In this table, the similarly obtained values for HSA are also included (see section 2.3.3).

From these experiments it is clear that the eluted apoHTF fractions contain bound vanadium complexes. The vanadium:apoHTF molar ratios determined in these fractions (3rd column of Table 2) are lower than those in the corresponding solutions added to the top of the size exclusion columns, the differences increasing with the increase in the initial $[V^{IV}O(acac)_2]$:apoHTF molar ratios. In fact, for the 1.01:1 ratio the difference between the ratios V:HTF in the added and eluted solutions is ≈11%, this meaning that the $V^{IV}O$-complex is quite strongly bound to apoHTF. For the 2.05:1 molar ratio, ca. 73% of vanadium remains bound to the protein, while for the 7.89:1 molar ratio only ca. 39% of total vanadium initially added remained bound to apoHTF. This suggests that up to a $[V^{IV}O(acac)_2]$:apoHTF molar ratio of ca. 2 the vanadium complex binds quite tightly to the protein, while higher amounts of $V^{IV}O$-acac species do not bind so strongly. Thus the equilibrium:

$$\text{Vanadium bound to apoHTF} \rightleftharpoons \text{Vanadium (not bound to apoHTF)} + \text{apoHTF} \quad (3)$$

is, in proportion, more shifted to the right as the $[V^{IV}O(acac)_2]$:apoHTF molar ratio of the solutions prepared increases, this indicating that the "first" two moles of vanadium bind to distinct sites (thus forming distinct and more tightly bound complexes) from those that start being "occupied" only when having higher molar ratios.

In these experiments, where the vanadium amount is determined by ICP-AES, no information may be obtained regarding which $V^{IV}O$-containing species bind to apoHTF. Notwithstanding, the data obtained by mass spectroscopy are compatible with those obtained with the size exclusion columns: a total of at least three $V^{IV}O$-moieties might bind to apoHTF. The mass spectrometric data suggests that when taking excess of $[V^{IV}O(acac)_2]$, two $[V^{IV}O(acac)^+]$ moieties may be bound to apoHTF residues, for example, of the Fe binding sites, as well as one $[V^{IV}O(acac)_2]$ (more weakly bound). We cannot rule out the possibility that the binding of VO-acac species to apoHTF might be non-covalent, but the pattern of results obtained and the fact that almost no binding was found for HSA indicates that at least two VO-acac species bind to apoHTF involving coordinative bonds.

Table 2. $[V^{IV}O(acac)_2]$:apoHTF and $[V^{IV}O(acac)_2]$:HSA molar ratios of the solutions prepared and applied to the top of size exclusion columns, and the same ratios determined on the fraction collected containing the protein.[a,b]

$[V^{IV}O(acac)_2]$:protein molar ratio before elution	Vanadium concentration (M) in the 1st eluted fraction[a]	Vanadium:protein molar ratio in the 1st eluted fraction[b]	Relative values (in %) of the V:protein molar ratios before and after elution
apoHTF			
1.01	$0.8(4)\times10^{-4}$	0.9	89%
2.05	1.4×10^{-4}	1.5	73%
4.02	1.9×10^{-4}	2.1	52%
7.89	2.9×10^{-4}	3.1	39%
HSA			
2.0	$<10\times10^{-6}$	<0.2	<10%
5.0	5.1×10^{-5}	≈0.5	≈10%

[a] The concentrations of vanadium in the first eluted fractions were determined by ICP-AES. [b] The concentration of apoHTF and of HSA in the eluted fractions was determined by UV absorption spectroscopy upon eluting samples only containing the protein. In the case of apoHTF the solutions applied on the top of the column were ≈140 μM and in the 1st eluted fraction were ≈94 μM; in the case of HSA they were 137.4 μM and in the 1st eluted fraction were ≈96.1 μM.

2.2.5. Electron Paramagnetic Resonance

Our present CD data clearly confirm that $V^{IV}O$-acac-apoHTF species do form in solutions containing $[V^{IV}O(acac)_2]$ and apoHTF, contradicting previous conclusions[29,44] mainly based on EPR spectroscopic measurements, where no $V^{IV}O$-acac-apoHTF species were identified. In studies with HSA[29,38] and with Immunoglobulin G[43] it was also reported that only $[V^{IV}O(acac)_2]$ (not bound to the proteins) is detected.

The EPR spectra for aqueous solutions of $[V^{IV}O(acac)_2]$ depict broad lines due to solute aggregation upon samples freezing. Addition of ≈2% of ethylene glycol favors glass formation and well-resolved spectra are obtained. Several solutions of $[V^{IV}O(acac)_2]$ in this work were made in DMSO and later diluted in buffers, the content of DMSO varying from 4 to 10%; the EPR spectra of frozen solutions of $[V^{IV}O(acac)_2]$ containing 2% of ethylene glycol or 4–10% of DMSO were identical. Figure SI-4-1 depicts examples of these EPR spectra and Table 3 summarizes the spin Hamiltonian parameters obtained. The spectra of $[V^{IV}O(acac)_2]$ in water was simulated considering either (i) axial symmetry and the presence of 2 species; or (ii) rhombic symmetry considering only one species. Although both simulations gave good fittings, the bandwidth in the low and high field regions is quite large, suggesting that 2 species coexist (see Figures SI-4-2 to SI-4–5 and discussion in SI section). Therefore, in Table 3 we consider the existence of two species. The spin

Table 3. Spin Hamiltonian parameters obtained for the systems $V^{IV}OSO_4$ and apoHTF and $[V^{IV}O(acac)_2]$ and apoHTF in this work and in previous publications. The present data were obtained by simulation of the experimental EPR spectra with the computer program of Rockenbauer and Korecz.[90]

System		g_x, g_y	g_z	A_x, A_y ($\times 10^4$ cm^{-1})	A_z ($\times 10^4$ cm^{-1})	g(iso), A(iso)
$V^{IV}O$-HTF species[26,29,30,32,84,88,89,91]	A		1.938 ± 0.002		168.5 ± 0.5	
$V^{IV}O$-HTF[29,30,84,89]	B		1.939 ± 0.003		171.0 ± 1.0	
$[V^{IV}O(acac)_2]$ in MeOH (axial)[51]		1.975 1.981	1.948	60.4, 56.2	166.8	1.968, 96.6
$[V^{IV}O(acac)_2]$ in MeOH[2]	A′ B′	1.978 1.976	1.946 1.948	55.4 60.0	168.5 164.6	1.967, 93.2 1.967, 94.6
$[V^{IV}O(acac)_2]$ in MeOH, this work		1.984 1.981	1.950 1.952	56 61	169 166	
$[V^{IV}O(acac)_2]$ in water or methanol, DFT calculations, this work				60, 62.6	167.3	
$[V^{IV}O(acac)_2]$ in water[65]	Major minor					1.970, 92 1.970, 97
$[V^{IV}O(acac)_2]$ in water[49]		1.977 1.970	1.946	51.4 56.1	166.5	
$[V^{IV}O(acac)_2]$ in water (containing 2% EtGlycol), this work[a]		1.985 1.982	1.955 1.957	55.2 59.3	168.0 167.5	
$[V^{IV}O(acac)_2]$ in water[2]		1.976 1.974	1.946 1.945	54.4 59.0	165.3 168.0	1.966, 91.3 1.964, 95.4
$[V^{IV}O(acac)_2]$ and apoHTF (4:1)[29]			1.948		166.8	
$[V^{IV}O(acac)_2]$:apoHTF 2:1 this work[b]	C Minor D Major	1.984 1.982	1.955 1.949	58.8 56.6	167.1 171.5	
$[V^{IV}O(acac)_2]$:apoHTF 4:1 C this work		1.984	1.956	58.7	167.4	

[a] EPR spectra of frozen solutions of $[V^{IV}O(acac)_2]$ containing 2% of ethylene glycol (EtGlycol) or 4-10% of DMSO are identical. [b] The EPR spectra of frozen solutions containing $[V^{IV}O(acac)_2]$ and apoHTF in the presence or absence of carbonate are identical (see Figure SI-5-1).

Hamiltonian parameters calculated theoretically using DFT methods and considering either water or methanol as solvent both yielded $A_z = 167.3 \times 10^{-4}$ cm^{-1}, thus giving good agreement with the experimental values obtained in this work or with those of Garribba et al.[49] and other authors.[2,51]

The EPR spectra of the solutions containing $[V^{IV}O(acac)_2]$ and apoHTF frozen ca. 10 min. and 24 h after preparation are identical (Figure SI-5-2). Figure SI-5-3 depicts X-band EPR spectra, measured at 77 K, of a solution of $[V^{IV}O(acac)_2]$ in water (containing ≈10% DMSO) and of solutions containing $[V^{IV}O(acac)_2]$ and apoHTF (2:1 and 4:1 molar ratios). Noteworthy is the observation that while the EPR spectra for solutions containing $[V^{IV}O(acac)_2]$:apoHTF molar ratios of 4:1 (typically the conditions used in the experiments of Garribba and co-workers[29,44]) are almost identical to those of $[V^{IV}O(acac)_2]$, that of the sample with 2:1 molar ratio differs significantly. This is emphasized in Figure 8, where an amplification of the high field range of the same spectra is depicted. The species designated by D (with $g_z = 1.949$; $A_z = 171.5 \times 10^{-4}$ cm^{-1}) differs from those of $[V^{IV}O(acac)_2]$. It resembles the spin Hamiltonian parameters of the $V^{IV}O$-apoHTF species B (Table 3), but the corresponding CD spectra differ significantly, thus species D should be assigned to a $V^{IV}O$-acac-HTF complex.

The spin Hamiltonian parameters determined for solutions containing $[V^{IV}O(acac)_2]$ in the presence or absence of apoHTF are quite similar, but not identical; they are also not much different from those obtained for the $V^{IV}O$-apoHTF system (Table 3). Regarding the identification of the $V^{IV}O$-acac-apoHTF species that form, namely if either $[V^{IV}O(acac)_2$-apoHTF] or [$V^{IV}O$(acac)-apoHTF] species form, it is not possible to indicate definite formulations from the EPR spectra measured. In fact, although frozen solution EPR spectra are an extremely useful tool to characterize and distinguish distinct $V^{IV}O$-species that may be present in a certain medium,[84–89] EPR spectra of frozen solutions may not be a totally reliable guide for judging the molecular structure of $V^{IV}O$-complexes,[51,84] particularly when several species may form which yield similar spin-Hamiltonian parameters, as is the case here (see also below).

The formation of [$V^{IV}O$(acac)(apoHTF)] species is akin of the formation of [$V^{IV}O$(acac)(L)] compounds. Such type of complexes have been often reported, some of them with molecular structure characterized by single-crystal XRD and with data of frozen solution EPR spectra (see for example, Figure 9). In most of the complexes depicted in Figure 9 the ligands L have donor atoms resembling those available in HTF, namely in its iron binding sites. Table SI-8.5-1 includes EPR spectroscopy data for several distinct systems containing $V^{IV}O$-acac species, with data including either $[V^{IV}O(acac)_2(L)]$ complexes (e.g. with L = Mepy or py)[51] or [$V^{IV}O$(acac)(L)] (e.g. with L = bzpy-tch[6] (**4**) and sal-dmen (**6**),[92] Figure 9), where the spin Hamiltonian parameters are quite similar, some of them involving the $acac^-$ ligand with one of the O_{acac} donor atoms bound *cis* to the O_{oxido}.

Considering complexes $[V^{IV}O(acac)_2(4\text{-Phpy})]$ (**3**) and $[V^{IV}O(acac)_2(py)]$ (**9**), while the DFT calculated energies of the *trans*- and *cis*-isomers in MeOH solution are similar (the *cis*-isomer is more stable than the *trans*-one by 3.3 and 7.5 kJ mol^{-1}, respectively), their corresponding theoretical A_z values are also almost identical, that is, 160.6×10^{-4} (**3**-*trans*), 161.2×10^{-4} cm^{-1} (**9**-*trans*), 159.5×10^{-4} (**3**-*cis*) and 159.7×10^{-4} cm^{-1} (**9**-*cis*). These values are lower by ≈4% than those observed experimentally for the system bearing $[V^{IV}O(acac)_2]$ and pyridine (165.5×10^{-4} cm^{-1},[51] Table SI-8.5-1), the latter being closer to the A_z value of the penta-coordinated complex $[V^{IV}O(acac)_2]$ ($165–168 \times 10^{-4}$ cm^{-1}, Table 3). The calculations also suggest that the coordination of Phpy or py to $[V^{IV}O(acac)_2]$ is not favorable thermodynamically, being both

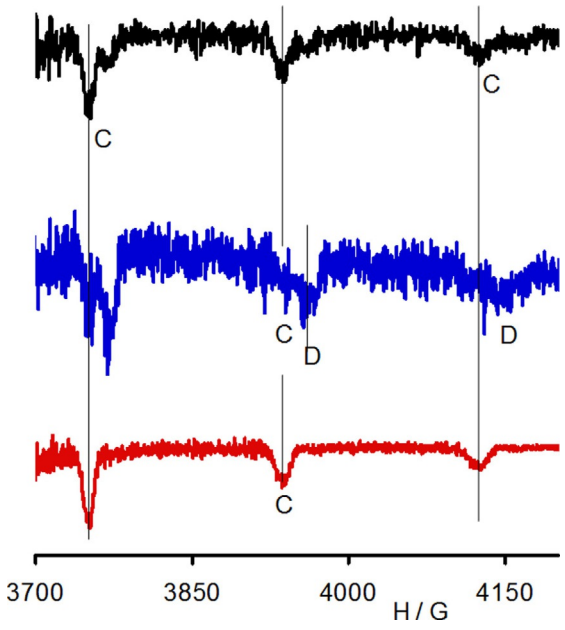

Figure 8. High field range of the 1st derivative EPR spectra of solutions of $[V^{IV}O(acac)_2]$ (black), or $[V^{IV}O(acac)_2]$ and apoHTF with 2:1 molar ratio (blue) and 4:1 molar ratio (red), recorded at 77 K. The vertical lines are inserted to better identify the position of the maxima. The full spectra are depicted in Figure SI-5-3.

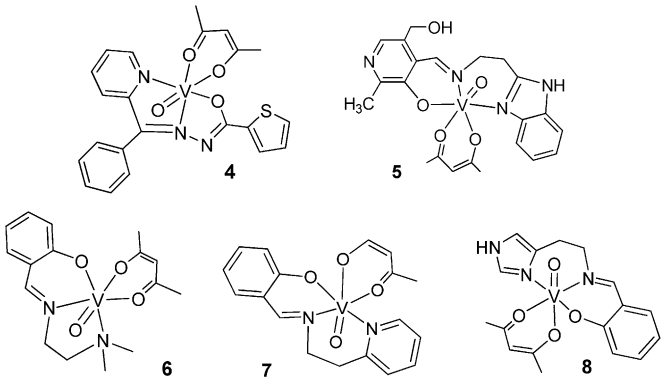

Figure 9. Several $[V^{IV}O(acac)(L)]$ complexes reported in the literature, some of them with spin Hamiltonian parameters closely resembling (see Table SI-8.5-1) those obtained for the $V^{IV}O$-acac-apoHTF system. For compounds **5**–**8** single-crystal XRD molecular structures were determined.

endothermic (by $\approx$21 kJ mol^{-1}) and endergonic (by 70.7–74.9 kJ mol^{-1}).

Comparison of the data included in Tables 3 and SI-8.5-1 allows stating that, the assignment of a particular formulation or concluding the non-formation of $V^{IV}O$-acac-apoHTF species, based on the solution EPR spectra measured for the $[V^{IV}O(acac)_2]$—apoHTF system, cannot be made reliably. Other techniques must also be used (e.g. CD, MS measurements, etc.) and the conclusions made must be compatible with all experimental results obtained.

The similarity of the spin Hamiltonian parameters of several $[V^{IV}O(acac)_2(L)]$ and $[V^{IV}O(acac)(L)]$ complexes and the CD and EPR spectra obtained for the $[V^{IV}O(acac)_2]$—apoHTF system lead us to state that the formation of $[V^{IV}O(acac)(apoHTF)]$-type species appears quite plausible. Thus, the EPR spectra obtained in this work may be considered compatible with the suggestion made above, that a significant fraction of the complexes formed in solutions of $[V^{IV}O(acac)_2]$ and apoHTF correspond to $[V^{IV}O(acac)(apoHTF)]$ species, such as the example depicted in Figure 10 A, where the $V^{IV}O$:acac molar ratio is 1:1 and the V^{IV} is bound to more than one chiral residue of apoHTF.

According to the data of Table 2, at least three $V^{IV}O$ centres may bind to apoHTF. If two bind to residues of the two iron binding sites (e.g. as the example of Figure 10 A), then it is plausible that at least one $[V^{IV}O(acac)_2]$ may be bound to apoHTF at a side group of an available imidazole, amino or carboxylate moiety of HTF residues (see Figure 10, **B-*trans*** and **B-*cis***). The formation of these $[V^{IV}O(acac)_2(apoHTF)]$ species resembles that of the many $[V^{IV}O(acac)_2(L)]$ complexes reported in the literature, for example, **2**–**8** and **3** (Figure 2, 9 and 10A), this by itself supporting the plausibility of their formation.

At this point it is also worth to mention that the immobilization of $[V^{IV}O(acac)_2]$ onto solid supports has been reported[15,95–97] and the binding established has been considered to involve: (i) hydrogen bonding between the pseudo π system of the $acac^-$ ligand and the silanol protons of the supports, and/or (ii) ligand-exchange with the formation of a covalent bond between the V centre and an O-atom from the support, (iii) interactions between the complex vacant orbitals and the π electrons of the polymer benzene rings of polystyrene supports,[97] (iv) Schiff base formation by condensation between the carbonyl group of the $acac^-$ ligand and the free NH_2 groups previously grafted onto the support's surface.[95] Namely, the immobilization of $[V^{IV}O(acac)_2]$ onto silica nanoparticles functionalized with 3-aminopropyltriethoxysilane (APTES) was reported to involve a covalent bond of the *N*-amino atom with the V^{IV} centre, as depicted in Figure 11.[15] This grafted complex was applied in the catalytic epoxidations and it could be recycled and reused four times, with similar catalytic activity and regioselectivity. This means that the bond established is strong enough for the complex to remain attached to the solid support.

Thus, whatever the correct formulation of these anchored $V^{IV}O$-acac species to solid supports, besides the $V^{IV}O$-acac-apoHTF species discussed above (probably bound to some of the amino acid residues of Fe binding sites), the formation of $[V^{IV}O(acac)_2(apoHTF)]$ complexes most probably also occurs, but correspond to weaker interactions. In these species, besides the monodentate coordination of donor atoms of available imidazole, amino or carboxylate moieties of HTF residues, probably several types of intermolecular interactions are also operating, for example, hydrogen-bond formation.

The formation of a Schiff base between -NH_2 of amino acid residues, for example, a lysine, and acac ligands probably does not occur, as no electronic transitions due to imine bonds were detected in the range 300–400 nm; additionally, the Gibbs free energy of the reaction depicted in Scheme 1 suggests that the process might not be thermodynamically favored.

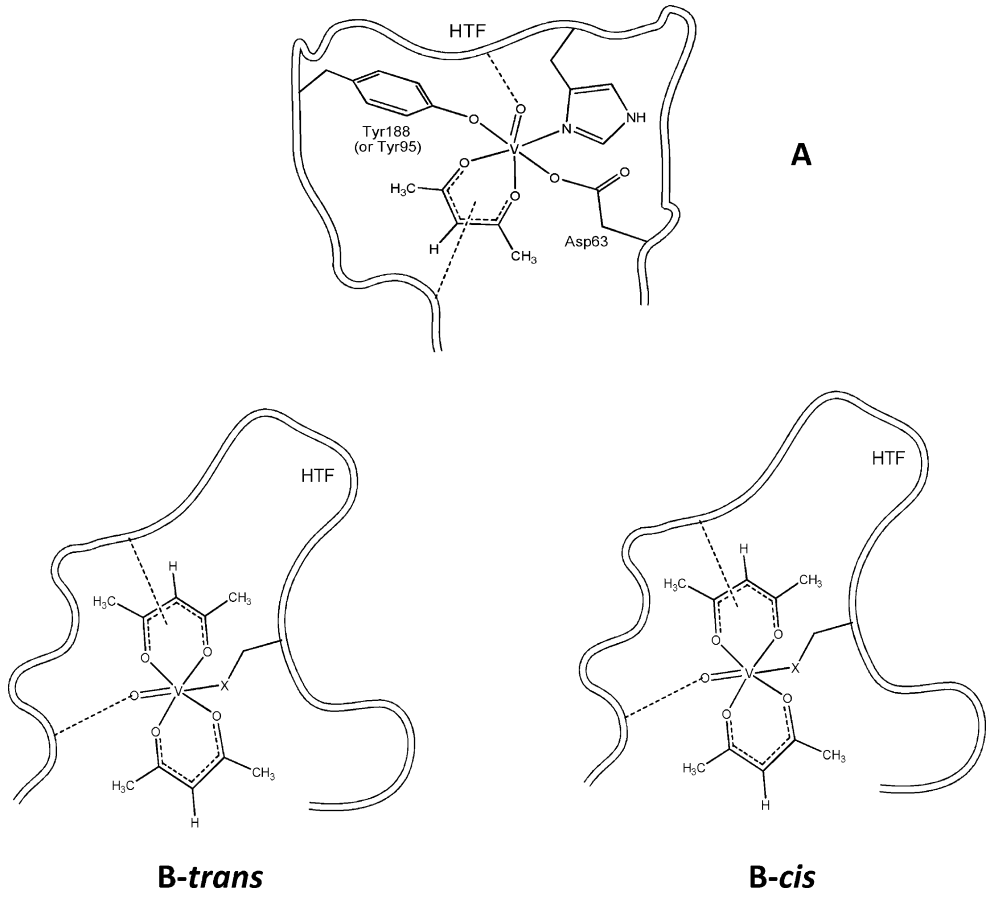

Figure 10. Sketches of types of binding of $V^{IV}O$–acac species to apoHTF. **A**: binding of $[V^{IV}O(acac)^{+}]$ to donor atoms of amino acid residues of apoHTF, belonging or not to the iron binding sites (here amino acids of residues from the *N*-lobe are specified); **B-*trans***: binding of a donor atom *trans* to O-oxido of $[V^{IV}O(acac)_2]$; **B-*cis***: binding of a donor atom *cis* to O-oxido of $[V^{IV}O(acac)_2]$. Atom X may be for example, an *N*-amino, *N*-imidazole or O-carboxylato. The insertion of dashed lines emphasize that hydrogen bonds or π-type bonds may be established between $V^{IV}O$-acac complexes and residues of apoHTF.

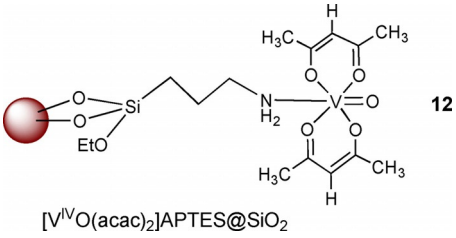

Figure 11. $[V^{IV}O(acac)_2]$ immobilized of onto silica nanoparticles functionalized with 3-aminopropyltriethoxysilane (APTES), as indicated in ref. [15].

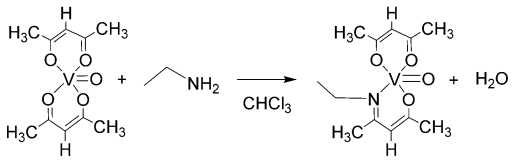

Scheme 1. Scheme modeling the reaction of $[V^{IV}O(acac)_2]$ with -NH_2 of an amino acid residue to form a Schiff base. The Gibbs free energy of this reaction in $CHCl_3$ solution calculated by DFT procedures is $+55.6\ kJ\,mol^{-1}$. The DFT calculated EPR spectroscopic parameters A_z, A_x and A_y for the complex with Schiff base are 163.4, 58.5, $57.7\times10^{-4}\ cm^{-1}$, respectively.

2.2.6. DFT calculations

To investigate the plausibility of coordination of the $[V^{IV}O(acac)^{+}]$ moiety to Tyr, Asp and His, the amino acid residues of the iron binding site of HTF, DFT calculations of the model complexes $[V^{IV}O(acac)(T)(A)(H)]^{-}$ (**1T**), $[V^{IV}O(acac)(T)_2(A)]^{2-}$ (**2T**) and $[V^{IV}O(acac)(T)_2(H)]^{-}$ (**3T**) (T = *p*-$EtC_6H_4O^{-}$, A = $EtC(=O)O^{-}$, H = 4-ethylimidazole) (Figure 12) were carried out for water solution. Model complexes **1T** simulate the binding of $[V^{IV}O(acac)^{+}]$ to one tyrosine, one aspartate and one histidine residues of apoHTF, while complexes **2T** and **3T** model the binding with two tyrosines and either one aspartate or one histidine residues. For each type of complex, all possible geometrical isomers were calculated (Figure 12). The results indicate that the isomer 6 of model complex **1T**, with the mutual *trans*-position of A and H, is the thermodynamically most stable one. For model complexes **2T**, the most stable one, isomer 3, bears two T ligands *trans* to each other. Finally, for model complexes **3T**, the most stable one, isomer 4, has the H and one of the T model ligands in the mutual *trans*-position. In all of these most stable isomers, one of the O-acac donors is *trans* to the O-oxido ligand. Other isomers of each type of model complexes are less stable by 3.3–25 $kJ\,mol^{-1}$.

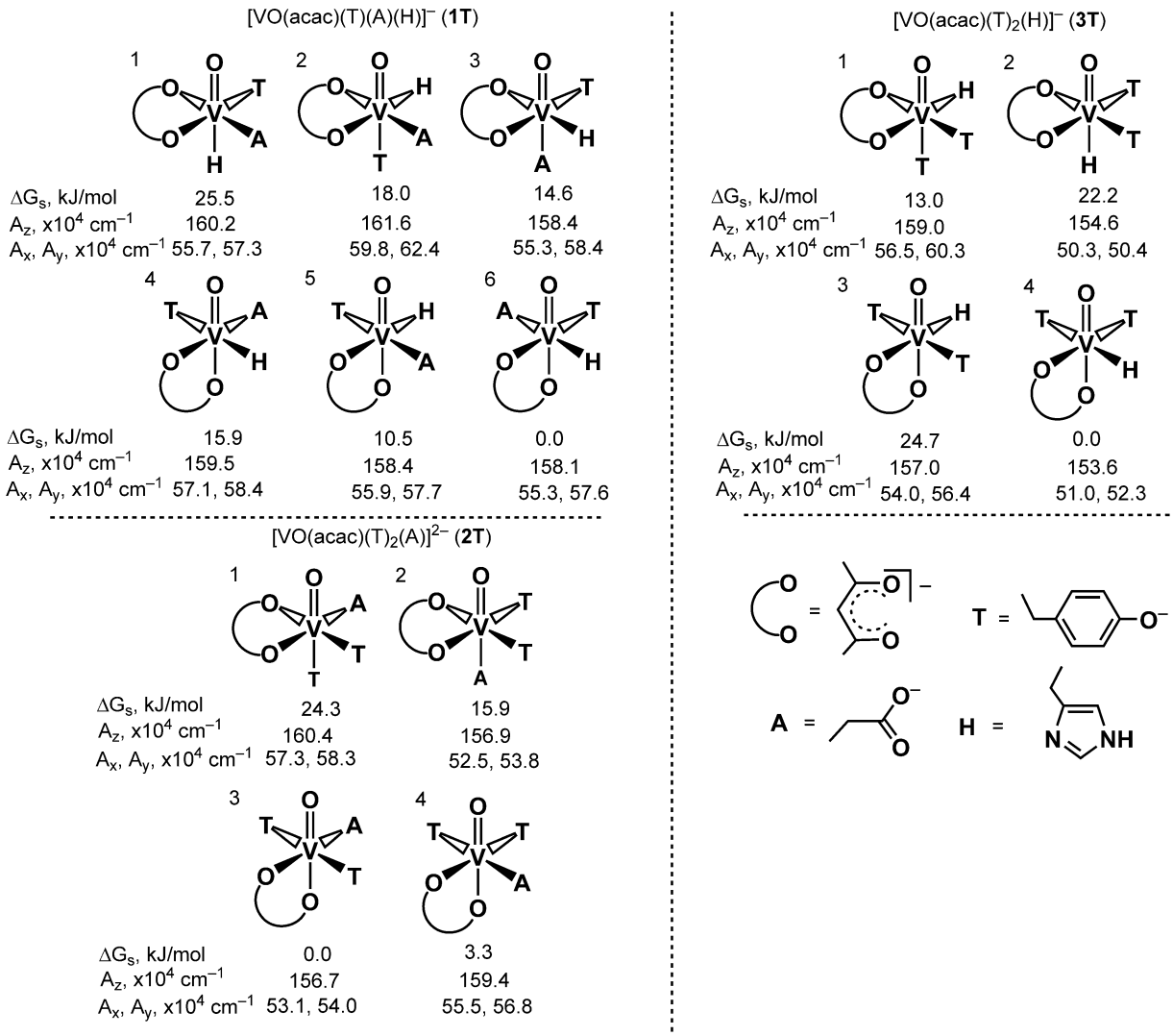

Figure 12. Calculated structures of complexes **1T-3T**. Gibbs free energies in water solution relative to the most stable isomer and A_x, A_y and A_z values are indicated.

The calculations also indicate that model complex **3T** is thermodynamically more stable than **1T**, the ΔG_s value of the reaction **1T** + T → **3T** + A being −22.6 kJ mol^{-1}. The stability of complex **2T** relative to **1T** or **3T** cannot be estimated with any reasonable accuracy due to different overall charge of these species. Note that in **1T-3T** the ligands are not linked with each other.

Taking into account the rather small energy difference of various geometrical isomers, the binding mode of [$V^{IV}O(acac)^+$] to apoHTF is conceivably controlled by the secondary structure of the protein and intermolecular interactions with groups from the protein, rather than by the thermodynamic stability of a particular ligand configuration in the metal coordination sphere. Noteworthy is the finding that in all these simulated [$V^{IV}O(acac)(L1)(L2)(L3)$] structures, those found more stable involve one of the O_{acac} donor atoms bound axially. It should also be emphasized that hydrogen bonds to for example, the O_{oxido} or O_{acac} atoms may change significantly the relative energies and the A_z values corresponding to calculated **1T-3T** model structures.

The calculated hyperfine coupling constants A_z for the various isomers of **1T-3T** are in the range of 153.6–161.6 × 10^{-4} cm^{-1} (Figure 12) and they are lower than the values found experimentally for the system [$V^{IV}O(acac)_2$] + apoHTF (Table 3). However, in similar structures including one water molecule bound equatorially, instead of for example, a O-Tyr donor atom, the corresponding A_z values increase by (3 to 6) × 10^{-4} cm^{-1} (Figure 13).

The calculated ΔH_s values of the reactions: [$V^{IV}O(acac)_2$] + T + A + H → $acac^-$ + **1T** (isomer 6) and $VO(acac)_2$ + 2T + H → $acac^-$ + **3T** (isomer 4) are significantly positive (62.8 and 41.0 kJ mol^{-1}, respectively) indicating that the formation of complexes **1T** and **3T** from $VO(acac)_2$ is thermodynamically unfavorable. This again suggests that the binding of [$VO(acac)^+$] to apoHTF should be stabilized also by intermolecular H-bonding rather than by simple coordination of T, A and H to the

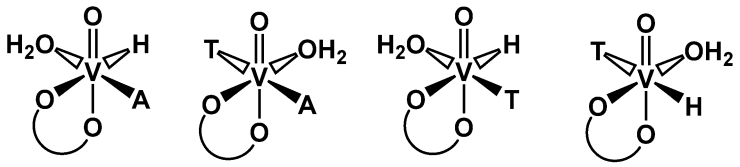

A_z, x10^4 cm^{-1}	165.0	160.8	159.8	159.9
A_x, A_y, x10^4 cm^{-1}	64.7, 63.2	59.4, 58.2	60.5, 56.8	61.8, 57.8

Figure 13. Calculated structures and spin-Hamiltonian parameters for some of the complexes of Figure 12, substituting equatorially bound O-Tyr donor atoms, by O_{water} donor atoms.

metal. These effects are not taken into account in the calculations corresponding to Figures 12 and 13, neither possible effects from rearrangement of the apoHTF conformation upon binding of VO-acac species. In the next section these effects are somewhat taken into account.

2.2.7. Modeling of the binding of VO-acac species to HTF

$V^{IV}O$ and various $V^{IV}O$-acac complex species, namely $[V^{IV}O(acac)_2]$, $[V^{IV}O(acac_2)(H_2O)]$, $[V^{IV}O(acac)(H_2O)_2]$ and $[V^{IV}O(acac)(H_2O)]$, were optimized at the PM7 semi-empirical level as implemented in MOPAC2016[98,99] and were checked against B3P86/6–311 g DFT geometries.[100] The *N*-lobe of HTF was modelled using (a) the closed conformation (PDB ID 1a8e),[101] (b) the oxalate-bound conformation (PDB ID 1ryo)[102] (3), which is not as tightly packed around the iron site as the closed conformation, as well as using (c) the open conformation (PDB ID 1bp5);[103] in the latter, the V atom was located at the geometric centre of the iron-coordinating residues (see experimental and SI sections).

No meaningful structures of $V^{IV}O$-acac complexes with the closed conformation of HTF (after removing the Fe^{III} and carbonate ions) were found due to the small volume available to bind these complexes. For the other protein forms, the most energetically favourable protein complexes were formed with the $[V^{IV}O(acac)(H_2O)_2]$ species. For the association of all $V^{IV}O$ complexes, after re-optimization of protein conformation, computed heats of formation with the open form of the protein is always energetically preferred when compared with the association with the oxalate-bound form. Table SI-10-1 includes the computed heats of formation for the various systems before carrying out the re-optimization of protein conformation. Table SI-10-2 includes these data after the re-optimization. Globally, it may be stated that the binding of either $[V^{IV}O(acac)^+]$ or $[V^{IV}O(acac)_2]$ correspond to favourable thermodynamic processes, but it should be noted that in these calculations entropy changes are not taken into account.

The modelling of the binding of the $[V^{IV}O(acac)^+]$ moieties correspond to lower computed heats of formation than those for the binding of $[V^{IV}O(acac)_2]$. In each structure refined the VO-acac complexes are tightly held in place by a large range of interactions, including water bridges, hydrogen bonds and metal cation-π interactions. Additionally, the processes where the lower energies were obtained gave rise to a type of binding of vanadium to a tyrosine residue which was not anticipated. In fact, in the structures refined, apart from the $V{=}O$ bond lengths of ca. 1.6–1.7 Å, and the binding to two O-acac atoms at ca. 1.7–1.8 Å, the V^{IV} is bound to the aromatic ring of a tyrosine, with V-C distances in the 2.30–2.40 Å range, resulting in half-sandwich complexes; this type of binding has been found for vanadocene(IV)-type compounds[105,106] (see more details in the SI section, namely Figures SI-10-1, -2 and -3). Coordinating residues, and other relevant residues in the vicinity of the ligands, involve the Fe-binding residues, Asp63, Tyr95, Tyr188, and His249, but also other protein residues, in particular Lys206, Ser125, Ala126 and Pro247, also participate in the ligand-protein interaction, which is in agreement with previous results on the VO interaction with the N lobe of hTF in the presence of carbonate.[104] However, the A_z values calculated for the model structures, upon freezing its coordinates similarly to what was done in [104] are rather low, ca. 141×10^{-4} cm^{-1}, so we rule out this type of binding of $V^{IV}O$-acac species.

The structure (model A, Figure SI-10-4) where in equatorial position are O-acac (at 1.9 Å), two O-atoms from Tyr188 (O at 1.9 Å) and Tyr95 (HO at 2.5 Å), O-carboxylate from Asp63 at (2.0 Å), and O-oxido and another O-acac axially, at 1.6 and 2.2 Å, respectively, correspond to $A_z = 162\times10^{-4}$ cm^{-1}, thus not far from experimental. The water molecule in the vicinity is at a 2.4 Å V-O_{water} distance and there is a hydrogen bond between the NH_3^+ of Lis296 and the O-oxido (H-O distance of 1.9 Å).

We are not stating that this particular structure (model A) is the one formed in the system: *N*-lobe of apoHTF + $[V^{IV}O(acac)_2]$, but instead that the binding of $V^{IV}O(acac)^+$ moieties to residues of the Fe-binding site can be modelled, the reaction corresponding to this process is thermodynamically favoured and may yield structures with A_z values not far from those of $[V^{IV}O(acac)_2]$ complexes.

2.2.8. Fluorometric assays

Intrinsic protein fluorescence is mainly due to tryptophan and tyrosine residues. Fluorescence assays have been used to monitor the binding of several compounds to proteins, namely to HTF and HSA. The study of the binding of $[V^{IV}O(acac)_2]$ to BSA by fluorometric measurements was reported before,[39] but not to HSA.

Tryptophan residues are the least common amino acids in proteins but normally dominate their fluorescence proper-

ties,[107–109] and are the most commonly used intrinsic fluorophores. The fluorescence emission from Trp residues is very sensitive to changes in local environment[110] and this sensitivity has been used extensively to monitor numerous biological processes. However, often it is not possible to pinpoint the precise causes of changes in the fluorescence yield, thus limiting the usefulness of the fluorometric measurements. If there is more than one Trp in a protein, as is the case of HTF, further complications arise when trying to interpret the changes in fluorescence at the molecular level. However, it was reported that emission from the *N*-lobe of HTF is dominated by Trp264.[108]

Except one study with vanadocene dichloride,[111] to our knowledge fluorometric techniques were not previously reported for studies of binding of vanadium compounds to HTF. The binding of $V^{IV}O$-complexes to apoHTF, namely at the iron binding sites, leads to the presence of the $V^{IV}O$-species not far from a Trp residue at each site; moreover, the hydrodynamic volume of the protein may change. Both these effects may change the fluorescence intensity.

Figure 14 depicts fluorescence emission spectra of the apoHTF-$[V^{IV}O(acac)_2]$ system, when using the excitation wavelength (λ_{ex}) of 295 nm. ApoHTF demonstrates strong fluorescence emission with a maximum at ≈322 nm. As the complex concentration increases the HTF fluorescence decreases; thus, the fluorescence quenching is concentration-dependent and apparently $[V^{IV}O(acac)_2]$ binds close enough to the tryptophan residues, namely Trp264, to quench their fluorescence. Under our experimental conditions, no fluorescence emission in the range 295–550 nm was displayed for the studied compounds and therefore there was not any interference with the fluorescence of apoHTF.

It is common to use fluorescence quenching measurements to evaluate binding constants of compounds to proteins. In the case of organic compounds, the conditions required for such methods to be reliable for use for this purpose have been discussed.[112,113] If these conditions are nor fulfilled, fluorescence quenching measurements should not be applied to evaluate binding constants of compounds to proteins, but in practice many studies are published without verifying the validity of the procedures. In the case of metal complexes there are further requirements that will be discussed below.

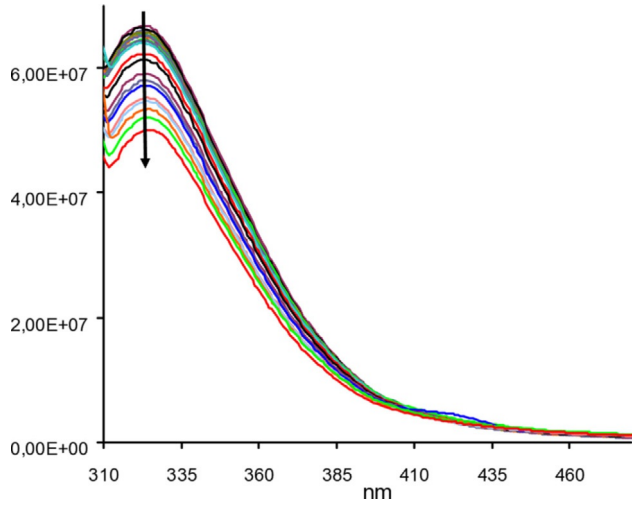

Figure 14. Variation of the fluorescence intensity of apoHTF upon addition of $[V^{IV}O(acac)_2]$. The apoHTF concentration was 1.02×10^{-6} M and that of $[V^{IV}O(acac)_2]$ was increased from 0 to 1.77×10^{-5} M, that is, from $[V^{IV}O(acac)_2]$:HTF: ratios from 1 to 17. Conditions: $T=298$ K, pH 7.4 (buffer) and $\lambda_{ex}=295$ nm. Concentration of the mother solution of $[V^{IV}O(acac)_2]$ added: 188 μM.

The methodology typically used in many publications was used in this work and is described in the SI section (SI-6); namely the fluorescence quenching measurements were made with a concentration of protein (apoHTF) of ca. 10^{-6} M, and varying the metal complex concentration from ca. ca. 10^{-6} to ca. 10^{-5} M (see Figure 14).

Upon applying the Stern–Volmer equation the corresponding quenching constant K_{SV} was obtained (Table 4). Following the typical calculation methodologies used in the literature, the quenching mechanism was considered to be static (due to binding of a VO-acac complex to apoHTF) and the binding constant K_{BC} given by equation 4, and number of binding sites (n) were determined (Table 4).

Table 4. Stern–Volmer constant (K_{SV}), R^2 (from SV plot), binding constant (K_{BC}), number of binding sites on the protein (n) and R^2 (from K_{BC} fitting) for the interaction of $[V^{IV}O(acac)_2]$ with HTF and HSA (see below).

Protein	10^{-4} K_{SV}(M^{-1})	R^2	10^{-4} K_{BC}(M^{-1})	n	R^2
HTF	1.9	0.993	1.05	1.15	0.995
HSA	3.7	0.952	0.023	0.61	0.977

$$n\ [V^{IV}O(acac)_2] + \text{protein} \rightleftharpoons \{[V^{IV}O(acac)_2]\}_n\text{-protein} \qquad (4)$$

When excitation was made at 280 nm (for which the other protein fluorophores, Phe and Tyr, may also be excited) a higher quenching % was obtained (45%), as well as a higher K_{SV} constant (3.9×10^4 M^{-1}). The calculated binding constant was: $K_{BC}=1.4\times10^4$ M^{-1}.

Considering the procedure described above and in the SI section (SI-6), from the fluorescence measurements we would conclude that $[V^{IV}O(acac)_2]$ is able to bind apoHTF, although the quenching of the fluorescence is only moderate. Around 30% quenching of the Trp fluorescence is observed, the K_{SV} being 1.9×10^4 M^{-1}, the binding constant K_{BC} estimated in these measurements being 1.0×10^4 M^{-1}.

Comments to the use of fluorescence quenching measurements to calculations of binding constants. The fluorescence and its quenching is a rather indirect measurement of the interaction of $[V^{IV}O(acac)_2]$ with apoHTF, as the Trp residues may not be close to the binding site responsible for the quenching effect, and there might be binding at sites which do not affect the fluorescence emission. Moreover, in the case of metal complexes, besides the requirements discussed in [112,113] for the validity of use of fluorescence emission to calculate binding constants, there are further aspects/issues related to the speciation of the systems at low concentrations of labile metal com-

plexes to which some attention should be given and are now discussed.

Figure 3 depicts a speciation diagram calculated for total $V^{IV}O$ and acetylacetone concentrations of 2 and 4 mM, respectively. It is clear that in the pH range 6–8 $[V^{IV}O(acac)_2]$ is the main V^{IV}-complex present in solution. However, if the concentration of $[V^{IV}O(acac)_2]$ is ca. 2 μM, close to the concentrations used for the fluorescence quenching measurements in the systems $[V^{IV}O(acac)_2]$ + apoHTF (and $[V^{IV}O(acac)_2]$ + HSA), the relative importance of most V^{IV}-species differs (see Figure SI-7-2). Namely, at pH 7.4 there are almost no $[V^{IV}O(acac)^+]$ or $[V^{IV}O(acac)_2]$ species in solution. At these low $[V^{IV}O(acac)_2]$ concentrations most of $V^{IV}O^{2+}$ is in the form of $[(VO)_2(OH)_5^-]$ and $[VO(OH)_3^-]$.[3,25]

Considering the system $[V^{IV}O(acac)_2]$ + apoHTF (or HSA) and the conditions used in the fluorescence quenching measurements in Figure 14 (apoHTF (1 μM) and $[V^{IV}O(acac)_2]$, varying the $[V^{IV}O(acac)_2]$ concentration from 1×10^{-6} M up to 10×10^{-6} M, at pH 7.4), and taking the binding constant of $[V^{IV}O(acac)_2]$ to apoHTF ($K_{BC}=10^4$) obtained from the fluorometric measurements (Table 4), it is clear in Figure 15 that no $V^{IV}O$-acac-apoHTF species exist in significant concentration. Thus, any effects observed on the fluorescence spectra are not due to $V^{IV}O$-acac-apoHTF species formed, but instead to the formation of $[V^{IV}O(apoHTF)]$ and $[(V^{IV}O)_2(apoHTF)]$ complexes.

It is thus concluded that the methodology used above leading to the values presented in Table 4 is not valid to determinate the binding constants of $[V^{IV}O(acac)_2]$ to apoHTF or to HSA. This conclusion may probably be equally applied to many other labile (and hydrolysable) metal complex—protein systems previously reported with binding constants determined by fluorescence quenching measurements. We do highlight that researchers should carefully check which species may be present at low protein and metal concentrations before applying these methodologies.

Even if a binding constant K_{BC} of 10^{12} is used for this system, possibly much higher than would be reasonable to expect, the speciation obtained (see Figure SI-7-3) indicates that in the conditions used for the fluorescence quenching measurements, it would also be not valid to apply the above mentioned methodology; in fact, in this case there would be at least 3 species contributing to the quenching of the fluorescence: $[V^{IV}O(apoHTF)]$, $[(V^{IV}O)_2(apoHTF)]$ and $[V^{IV}O(acac)_2(apoHTF)]$, not simply the last one.

2.3. Interaction of $[V^{IV}O(acac)_2]$ with human serum albumin

2.3.1. Circular dichroism and EPR spectroscopies

As mentioned above, the binding of $[VO(acac)_2]$ to BSA was studied by ITC and fluorescence spectroscopy.[2,39] Namely, it was reported that a 1:1 adduct is formed between $[V^{IV}O(acac)_2]$ and bovine serum albumin (BSA), with dissociation constants (K_d) of 2.6×10^{-7} (ITC) and 6.1×10^{-7} (fluorescence),[39] these correspond to binding constants ($1/K_d$) of 3.8×10^6 and 1.6×10^6, respectively; this was considered an important factor for its biological activity in vivo, particularly its insulin-enhancing effect.[2]

The binding of $V^{IV}O^{2+}$ to human serum albumin was studied by several techniques, namely by EPR and ENDOR spectroscopies,[27,38,44,89,115,116] CD and visible absorption.[116] The results show that $V^{IV}O$ occupies two types of binding sites in HSA; in one of the sites the resulting $V^{IV}O$-HSA complex has a weak CD signal in the visible and its EPR spectrum may be easily measured; this was assigned to amino acid side chains of the amino terminal site, Asp-Ala-His-, known as ATCUN site.[116] The other binding site depicts stronger signals in the CD in the visible range, but has a hardly measurable EPR spectrum; it was assigned as involving residues of the multi metal binding site (MBS) of HSA.[116] Studies with fatted and defatted albumin showed[116] that the binding of fatty acids decrease the ability of $V^{IV}O$ to bind albumin.

Figure 16 depicts CD spectra measured with solutions containing $[V^{IV}O(acac)_2]$ and defated HSA in the visible range. It is not clear if $\Delta\varepsilon\neq0$ are obtained at all; if yes, the bands are extremely weak. Even using higher $[V^{IV}O(acac)_2]$:HSA ratios no clear bands were recorded. Zn^{II}-complexes do not absorb radi-

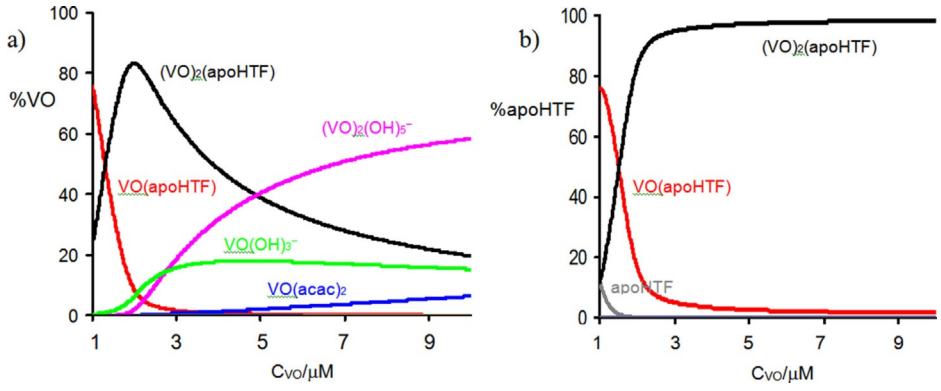

Figure 15. Speciation diagrams for the system apoHTF (1 μM) and $[VO(acac)_2]$, at pH 7.4, varying the total $[V^{IV}O(acac)_2]$ concentration (C_{VO}) from 1×10^{-6} M up to 10×10^{-6} M (see text of SI section), and taking the binding constant of $[VO(acac)_2]$ to apoHTF obtained in the fluorescence quenching measurements ($K_{BC}=10^4$) by applying the typically used methodologies. The binding constants of $[V^{IV}O(apoHTF)]$ and $[(V^{IV}O)_2(apoHTF)]$ are from [31], are valid at pH 7.4. The formation constants for the system $V^{IV}O^{2+}$ + acac are from [4] and the hydrolytic constants for $V^{IV}O^{2+}$ from [3,25]. (a) Distribution of species containing $V^{IV}O$, (b) Distribution of species containing apoHTF.

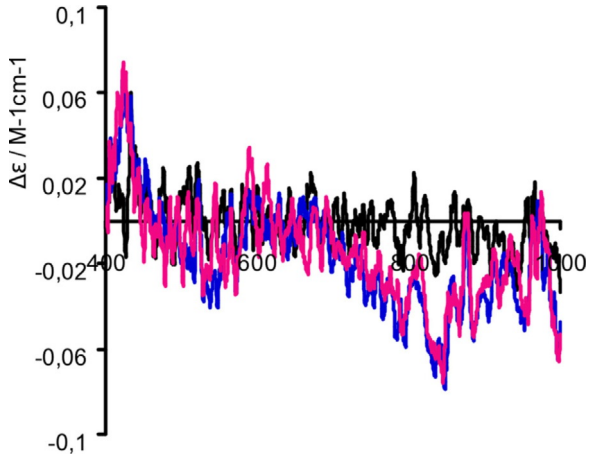

Figure 16. CD spectra of solutions containing $[V^{IV}O(acac)_2]$ and HSA (600 μM) in PBS buffer of pH 7.4. HSA (black spectrum), $[V^{IV}O(acac)_2]$:HSA (2:1, immediately after addition of $[V^{IV}O(acac)_2]$, blue spectrum) and the same solution after ca. 1 h (red). An optical path of 20 mm was used.

ation in the 400–1000 nm range and do not have unpaired electrons; therefore they are both CD and EPR silent. The Zn^{2+} ions bind strongly to the MBS binding site of HSA, so if any $V^{IV}O$-acac-HSA species binds at this site, if a Zn^{II} salt is added they will be removed from it.[116–118] Upon addition of $ZnCl_2$ to a solution of $[V^{IV}O(acac)_2]$ and HSA with a molar ratio of 2, the very weak bands apparently observed in Figure 16 in the 700–900 nm range are no longer seen; this could suggest that Zn^{2+} ions are substituting $V^{IV}O$-acac species bound at the MBS site; however, in all CD spectra the signal-to-noise ratio is so low that no definite conclusion can be made. The EPR spectra of solutions containing $[V^{IV}O(acac)_2]$ and HSA are depicted in Figures SI-5-4 and -5, as well as those recorded upon additions of a solution of $ZnCl_2$ so that Zn^{II}:HSA molar ratios of 1 and 2 are obtained. No clear difference may be detected in the EPR spectra of the frozen solutions of $[V^{IV}O(acac)_2]$ or $[V^{IV}O(acac)_2]$ and HSA containing or not Zn^{2+} ions. If any $V^{IV}O$-species were bound at the MBS site before the addition of $ZnCl_2$, the corresponding amount was small.

Globally, we may conclude that the EPR and CD spectroscopic data do not clearly rule out or confirm the presence of $V^{IV}O$-acac species bound to HSA; if the binding takes place, probably these correspond to $[V^{IV}O(acac)_2(HSA)]$ complexes involving monodentate coordination of an *N*-amino, *N*-imidazole or O-carboxylate from amino acid residues of HSA, otherwise much stronger CD spectra would be measured, as was the case of $V^{IV}O$-maltolato complexes.[117]

2.3.2. Use of size exclusion columns.

To further confirm the binding of $[V^{IV}O(acac)_2]$ to HSA, similarly to what was done above for apoHTF solutions containing HSA (ca. 137 μM), and two different amounts of $[V^{IV}O(acac)_2]$ were prepared, corresponding to the molar ratios 2 and 5, and eluted with tris buffer solution through desalting columns (PD-10 size exclusion columns, see SI section); the eluates of the first eluted fractions were analyzed by ICP-AES. The dilution effect (≈70%) was determined taking into account the absorbance of an HSA solution before and after eluting it, in experiments with no addition of $[V^{IV}O(acac)_2]$. Results of the ICP-AES analysis are included in Table 2.

The binding of $[V^{IV}O(acac)_2]$ to HSA is weak, thus it might happen that part of the $[V^{IV}O(acac)_2]$ initially bound to HSA was lost during elution through the size exclusion column, but clearly this data indicates that in solutions containing $[V^{IV}O(acac)_2]$:HSA molar ratios of 5, not more (most probably less) than one $V^{IV}O$-(acac) moiety is bound to each protein molecule.

2.3.3. Fluorometry experiments

While BSA has two Trp residues, HSA has only one. The intrinsic fluorescence of HSA is mainly due to the Trp214 residue, because of the very low quantum yield of the Phe and Tyr residues.[119,120] When the excitation wavelength (λ_{ex}) of HSA is selected at 280 nm both Trp and Tyr residues contribute to the fluorescence emissions. However, at $\lambda_{ex}=295$ nm, the emission observed is only due to Trp214 which displays a strong fluorescence emission peak with $\lambda_{max}\approx330$ nm.[119]

Under our experimental conditions, no fluorescence emission in the range 295–550 nm was displayed for the studied compounds and therefore there was not any interference with the Trp214 fluorescence of HSA. Figure 17 depicts fluorescence

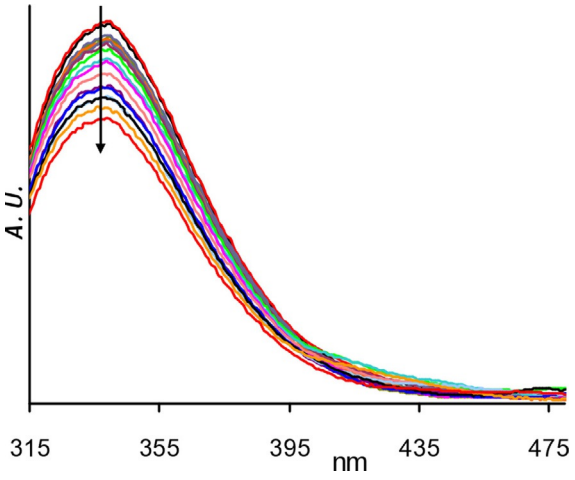

Figure 17. Fluorescence emission spectra measured for a solution of HSA and upon adding $[V^{IV}O(acac)_2]$. The initial concentration of the HSA solution was 1.03×10^{-6} M and that of $[V^{IV}O(acac)_2]$ was increased from 0 to 1.53×10^{-5} M (from $[V^{IV}O(acac)_2]$:HSA ratios 1 to ≈15). Conditions: $T=298$ K, pH 7.4 and $\lambda_{ex}=295$ nm. The arrow indicates the $[V^{IV}O(acac)_2]$ concentration increase. The concentration of the solution of $[V^{IV}O(acac)_2]$ added was ≈234 μM, and the maximum amount of DMSO present was ≈1.2%.

emission spectra at $\lambda_{ex}=295$ nm of a solution of HSA (ca. 1 μM) and upon additions of a solution of $[V^{IV}O(acac)_2]$. Under these conditions HSA has fluorescence emission with maximum intensity at ≈338 nm. As the $[V^{IV}O(acac)_2]$ concentration increases the HSA fluorescence decrease; thus the fluorescence quenching is concentration-dependent and probably at least

part of the bound $[V^{IV}O(acac)_2]$ does it close to the Trp residue. However, after addition of ca. 5 mole equivalents of $[V^{IV}O(acac)_2]$, only ≈12% quenching is observed and ≈21% after addition of ≈15 mole equivalents, Figure SI-6-4.

We followed a similar methodology to the one applied in the $[V^{IV}O(acac)_2]$-apoHTF system, to obtain the Stern–Volmer constant and a binding constant of $[V^{IV}O(acac)_2]$ to HSA (see SI-section), and the results are shown in Table 4. However, as explained above, this methodology is not reliable or valid to obtain the binding constant in this system (and in many other systems reported in literature), and we include this information in this text to highlight this fact.

2.4. Human cells studies: intracellular distribution of $[V^{IV}O(acac)_2]$

The cytotoxic activity of $[V^{IV}O(acac)_2]$ was evaluated in the A2780 ovarian cells within the concentration range 0.1–100 μM using the colorimetric MTT assay. The complex presented moderate cytotoxic activity with an $IC_{50} = 66 \pm 18$ μM, after 24 h incubation with the cells (Figure SI-12-1).

The IC_{50} value (66 μM) was the concentration of $[V^{IV}O(acac)_2]$ selected to carry out intracellular distribution studies. As depicted in Figure 18 more than 60% of complex is retained in the membrane, where large complexes of proteins act to carry out vital cellular processes; this corresponding to ca. 18.5 ng of V/ million A2780 cells. Only a small percentage was retained in the nucleus, an interesting result taking into consideration the complex remarkable nuclease activity of $[V^{IV}O(acac)_2]$ using plasmids (naked DNA).[20,21]

Globally the total amount of vanadium analyzed by ICP-MS in the A2780 ovarian cells after 24 h of incubation with $[V^{IV}O(acac)_2]$ is low (about 30% or less of those of Cu and Zn amounts found in the same study, carried out with other types of complexes),[121] and more than 60% is localized on its membrane. The nature of the V-species present either in the membrane or in each of the cells' compartments is not known, and probably the amount found in the nucleus is too low to affect it.

The cells were cultured in RPMI supplemented with 10% fetal bovine serum (FBS), and exposed for 24 h to the complex. Fetal serum albumin, is one of the major components of FBS, and neither this protein nor HSA have specific binding sites for vanadium, thus we would expect rather similar transport capacity. Thus, this study suggests (at least for the A2780 ovarian cells), that albumins are not efficient transporters of $[V^{IV}O(acac)_2]$, for its uptake inside the cells. However, the amount of vanadium analyzed in the membranes is enough to affect significantly their metabolism. It is known that for example, membranes contain several types of relevant proteins, and the binding of V-species may change/inhibit their biological function.

3. Conclusions

$[V^{IV}O(acac)_2]$ (**1**), is one of the most remarkable vanadium compounds and found uses in multiple areas. Namely it has been suggested as a prospective drug for the treatment of diabetes, cancer and in tumor diagnosis. The understanding of how it is transported in blood is of major importance to establish its pharmacokinetics and pharmacodynamics.

Previous reports addressing the interactions between $[V^{IV}O(acac)_2]$ and plasma proteins are contradictory,[2,29,43–45] but have agreed in the conclusion that $[V^{IV}O(acac)_2]$ does not bind to human serum apotransferrin. In this work we report circular dichroism and MALDI-TOF data that clearly confirms that $V^{IV}O$-acac species bind to human serum apo-transferrin. The EPR spectra measured, SAXS data and DFT calculations corroborate the plausibility of this conclusion.

Analysis of apoHTF and vanadium contents of samples containing $[V^{IV}O(acac)_2]$ and apoHTF upon elution through size exclusion columns confirm that up to three $V^{IV}O$-acac species may bind to apoHTF. Similar studies carried out for the $[V^{IV}O(acac)_2]$-HSA system did not confirm or rule out binding to albumin, but the interactions of $[V^{IV}O(acac)_2]$ are much weaker with HSA than with apoHTF. For example, when using $[V^{IV}O(acac)_2]$:HSA ratios of 5, significantly less than one vanadium containing complex binds to HSA.

Previous reports[29,43–45] on the non-binding of $[V^{IV}O(acac)_2]$ to apoHTF explained by the stability of $[V^{IV}O(acac)_2]$, or the absence of water molecules coordinated in the equatorial position to be replaced by donor groups of amino acid residues, or inability of this binding, are contradicted by the numerous previous reports of this type of binding in solution, by the several

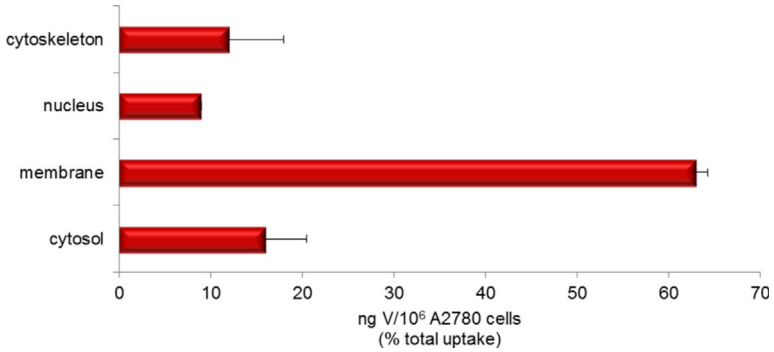

Figure 18. V content in the A2780 subcellular fractions after 24 h exposure to the complex at a concentration equivalent to the IC_{50} value (66 μM). Results are expressed as total vanadium accumulation in ng per million cells.

reported molecular structures determined by single-crystal XRD where such binding, forming either $[V^{IV}O(acac)_2(L)]$ or $[V^{IV}O(acac)(L)]$ complexes, have been confirmed. Additionally there are several publications of $[V^{IV}O(acac)_2]$ bound to solid supports and used as heterogenized catalysts, further attesting the plausibility of the formation of VO-acac-apoHTF complexes.

DFT calculations with $[V^{IV}O(acac)(L1)(L2)(L3)]$ complexes, where L1-L3 are models of His, Tyr and Asp residues, suggest that the (O_{axial}, $O_{equatorial}$) binding of $acac^-$ is preferred over the ($O_{equatorial}$, $O_{equatorial}$) type of binding. Additionally, DFT calculations suggest that, besides the coordination bonds established, probably the VO-acac-apoHTF species formed are stabilized by intermolecular interactions with amino acid residues from the protein. This is confirmed in modeling calculations of the binding of $V^{IV}O(acac)^+$ species to amino acids of the *N*-lobe of apoHTF.

Speciation calculations done for solutions with low concentrations of apoHTF (ca. 1–2 μM) and of $[V^{IV}O(acac)_2]$ (ca. from 1 to 17 μM), typical of fluorescence studies to evaluate the binding of metal complexes to HTF or albumin, rule out the possibility of using these methodologies to calculate the binding constants of $[V^{IV}O(acac)_2]$ to these proteins. We predict that similar conclusions may be extrapolated to many other complexes involving labile and hydrolysable metal ions, particularly those that bind strongly to serum proteins such as Cu^{II}, Zn^{II} and Fe^{III}. Globally, these speciation considerations also indicate that under physiological conditions, thus at low $[V^{IV}O(acac)_2]$ concentrations, ca. 10 μM or lower, most of the vanadium is bound to transferrin as $V^{IV}O$-[31,32] or V^{III}-HTF[30,33,37,122–124] species without the original $acac^-$ ligands. At higher $[V^{IV}O(acac)_2]$ concentrations and equivalent amounts of apoHTF, our data indicates that $[V^{IV}O(acac)^+]$ moieties bind to apoHTF involving coordination of V^{IV} to some of the Fe-binding site residues.

If $[V^{IV}O(acac)_2]$ is administered orally, certainly vanadium speciation in the gastrointestinal tract will change significantly and most probably vanadium and acetylacetone will reach the blood separately.[2,17,124] However, if the drug is administered by injection (or encapsulated), $[V^{IV}O(acac)_2]$ may then reach the blood maintaining its integrity. In either case this would not affect the final conclusions of the present study regarding the binding of $[V^{IV}O(acac)_2]$ to serum proteins.

In the intracellular distribution determination of $[V^{IV}O(acac)_2]$, evaluated in the human A2780 ovarian cancer cells at IC_{50} concentration (66 μM) for 24 h, the total vanadium up-taken is relatively low (when compared to Cu- and Zn-compounds examined in the same cells) and ≈63% of the vanadium analyzed by ICP-MS was found in the membrane, ≈9% in the nucleous, ≈12% cytoskeleton and ≈16% in the cytosol. The incubation medium in these studies also contained ca. 35 μM of fetal serum albumin, thus we would expect rather similar transport capacity as that of HSA". Thus, this study suggests, at least for the A2780 ovarian cells, that albumins are not efficient transporters of $[V^{IV}O(acac)_2]$ for its uptake inside the cells.

Experimental Section

4.1. Preparation of solutions

Millipore water was used for the preparation of solutions of the complexes for studies and buffer solutions. The water was produced using a Mili-Q water purification system.

Buffer solutions. Almost all measurements were carried out in aqueous buffered media. Phosphate Buffered Saline (PBS) from Sigma–Aldrich was used whenever stated: one tablet dissolved in 200 mL of Millipore® water yields 0.01 M phosphate buffer, 0.0027 M potassium chloride and 0.137 M sodium chloride, pH 7.4, at 25 °C. Hepes buffer. The composition of the Hepes buffer used is 50 mM Hepes (Sigma–Aldrich), 25 mM carbonate added as $NaHCO_3$ (Sigma–Aldrich), 1 mM phosphate added as $NaH_2PO_4{\cdot}H_2O$ (Merck) and 0.20 mM KCl (Merck). This buffer system was adjusted to a pH of 7.4 using concentrated KOH. The composition of the Tris buffer used is 0.10 M Tris and 50 mM $NaHCO_3$. This buffer system was adjusted to pH 7.4 using concentrated HCl.

Protein solutions. apoHTF (ATF2011-07; >95%), was purchased from Akron™ bio tech; fatty acid and globulin free human serum albumin (Sigma Aldrich, A3782, ≥99%), lyophilized powder with a molecular mass of 67 kDa was used. Human apo-transferrin solutions were prepared by dissolving the protein in buffer at pH 7.4. The solutions were allowed to stand for at least 1 h to allow equilibration. During this period they were gently swirled without strong agitation. The concentration of apoHTF solutions were determined by measuring the absorbance at 280 nm using an extinction coefficient of 92300 $M^{-1}cm^{-1}$,[31,125,126] and for albumin it was 36850 M^{-1} cm^{-1}.[31,127] Normally nitrogen gas was bubbled through all solutions prior to use for measurements with V^{IV}-complexes to displace any oxygen that may be present.

$[V^{IV}O(acac)_2]$ solutions. $[V^{IV}O(acac)_2]$ was purchased from Fluka® Analytical. Stock solutions were freshly prepared by dissolution in either DMSO or MeOH, and this was diluted in water or buffer for further use. Normally the amount of organic solvent present in the described experiments was 1–4%.

4.2. Desalting procedure with size exclusion columns.

PD-10 Desalting Columns containing Sephadex™ G-25 Medium, a size exclusion packing, were purchased from GE Healthcare, and used as recommended, namely the equilibration and elution procedures. Several $[V^{IV}O(acac)_2]$:protein (in tris buffer (0.10 M) containing Na_2CO_3 (2.5×10^{-2} M) molar ratios were used. Solutions were allowed to equilibrate for 10–20 minutes (under N_2 atmosphere). The dilution effect was determined by passing the protein samples and measuring their absorption at 280 nm before and after elution. In 5 mL volumetric flasks, to each protein solution (≈1.4×10^{-4} M) adequate volumes of $[V^{IV}O(acac)_2]$ (ca. 3×10^{-2} M) in DMSO were added to obtain the desired $[V^{IV}O(acac)_2]$:protein ratios. The first component to elute from these size exclusion columns is the protein, which may (or may not) contain bound vanadium-complexes. The protein-metal solutions collected from these exclusion columns were used to evaluate the vanadium content by ICP-AES, using a Horiba Jobin–Yvon apparatus, model Ultima.

4.3. Spectroscopic and mass spectrometric measurements

Ultraviolet-visible absorption spectroscopy. All UV/Vis absorption spectra were recorded with PerkinElmer Lambda 35 spectrophotometer. Quartz SUPRASIL® cells from Hellma® Analytics of either 1 mm, 2 mm, 10 mm or 20 mm optical path were used in the experiments.

Circular dichroism spectroscopy. CD spectra were recorded on a Jasco J-720 spectropolarimeter either using the usual photomultiplier (200–800 nm range) or with a red-sensitive photomultiplier (EXWL-308) in the 400–1000 nm range. The measurements were normally carried out at ≈25 °C using either a 20 mm (chamber volume ≈5.0 mL) absorption cells from Hellma®, or a Macro Suprasil® 3.5 mm I.D. ×50 mm cylindrical quartz cell (Jasco Parts Center, CQ3-50, chamber volume ≈800 μL),[78] or a 2 mm cell (chamber volume ≈600 μL) made of Quartz Suprasil® from Hellma® Analytics.

Electron paramagnetic resonance (EPR) spectroscopy. The first derivative X-band EPR spectra of the frozen solutions (frozen in liquid nitrogen) were recorded on a Bruker ESP 300E spectrometer at 77 K. The ESP 300E spectrometer was operated at ≈9.51 GHz with a frequency modulation of 100 KHz. The samples (250 μL) were placed in 3 mm quartz tubes (Wilmad 707-SQ-250M) and frozen in liquid nitrogen. The calibration of the magnetic field frequency was done using DPPH (2,2-diphenyl-1-picrylhydrazyl) as standard. While keeping the resolution at 4096 points, the microwave power was adjusted to 20 dB and the receiver gain was set between 4.5×10^4 and 7.9×10^4. To improve the signal-to-noise ratio 5 to 10 scans of each sample were accumulated.

Fluorescence spectroscopy. The fluorescence spectra were obtained on a Fluorolog® Horiba Jobin Yvon Spectrofluorometer with single proton counting controller—FluoroHub from Horiba Scientific™. The samples were excited either at the wavelength of 280 nm (slit width 5 nm) and the emission spectra were measured in the 290–500 nm range, or at 295 nm (slit width 9 nm) with the emission spectra measured in the 305–515 nm range. All measurements were done in 10 mm fluorescence quartz cells from Hellma® Analytics with the chamber volume of ≈3.50 mL at room temperature.

Electrospray mass spectrometry (ESI-MS). A 500-MS Varian Ion Trap Mass Spectrometer was used to measure ESI-MS spectra of solutions in both positive and negative modes. The mass spectrometer was operated in the ESI negative or positive ion mode, typically with the following optimized parameters: ion spray voltage, −4.5 kV; capillary voltage, −20 V; tube lens offset, −124.99 V, sheath gas (N_2), 20 arbitrary units (negative mode); ion spray voltage, 5 kV; capillary voltage, 5 V; tube lens offset, 63 V, sheath gas (N_2), 20 arbitrary units (positive mode); capillary temperature, 275 °C. Spectra typically correspond to the average of 20–35 scans, recorded in the range between 100–600 Da.

Matrix-assisted laser desorption/ionization time-of-flight mass spectrometry (MALDI-TOF). Mass spectra were obtained using a Bruker Daltonics Ultraflex MALDI TOF/TOF Mass Spectrometer operating in linear mode with positive ion extracting at 25 000 V and a pulsed ion extraction of 480 ns. Each final spectrum was the accumulated result of at least 1000 laser shots that were obtained from 10 different manually selected regions of the same sample, over a range of 14 000–100 000 Da. Prior to calibration, the spectra were processed with Compass 1.3 using smoothing and baseline subtraction for reproducible peak annotation. The spectra were externally calibrated using of 50 pmol of albumin from bovine serum ($[M+H]^+$ 66,430).

4.4. Small Angle X-ray Scattering (SAXS)

4.4.1. Sample preparation

Human serum apo-transferrin (apoHTF), from Sigma–Aldrich, was dissolved (20 mM Tris-HCl pH 8, 20 mM sodium carbonate and 200 mM sodium chloride) to a concentration of 6 mg mL^{-1}. A first sample of native apoHTF (500 μL) was then passed through a PD-10 MiniTrap G-25 column according to the previously reported procedure.[26] A second sample of apoHTF (500 μL) was incubated with a 30 times molar equivalent excess of $[V^{IV}O(acac)_2]$ at room temperature; after one hour of incubation, the excess of unbound ligand was removed using PD-10 MiniTrap G-25 column. In both samples, a final protein concentration of 3 mg mL^{-1} was obtained for a 1:2 diluted sample.

4.4.2. Data collection and processing

The two samples, native apoHTF and apoHTF-$[V^{IV}O(acac)_2]$, were analyzed by SAXS immediately after passing through PD-10 MiniTrap G-25 columns. SAXS data were collected at beamline BM29 (ESRF, Grenoble, France) using a robotic sample changer.[128,129] Ten frames of one second each were collected and all the measurements were done at 277 K. Different protein concentration ranges were used: 3 to 0.19 mg mL^{-1} for both samples. Data were reduced and analyzed using Scatter (Diamond Light Source, UK) and the ATSAS suite.[80] Each experimental frame was inspected for radiation damage; these frames were removed from further consideration and not used for buffer subtraction. Theoretical SAXS curves were calculated using CRYSOL.[82] Real space inversion obtain the P(r) function (pair distance distribution function) was carried out in Scatter. The P(r) function is the Fourier transform of the scattering pattern, and represents a histogram distances between all possible pairs of atoms in a structure. An ensemble of seven low resolution envelope models were generated from the P(r) function in DAMMIF,[130] and then subject to averaging and filtering with DAMAVER and DAMFILT.[131] The output from DAMFILT was then passed to DAMMIN as a start model for final refinement against the experimental curve. Other details are given in the SI section (SI-9).

4.5. Spectroscopic studies with solutions of $[V^{IV}O(acac)_2]$ and monodentate ligands

4.5.1. Absorption spectra of solutions of $[V^{IV}O(acac)_2]$ and monodentate ligands

For these studies an aqueous solution of $NaHCO_3$ was prepared and a controlled volume of HCl (1.0 M) was added, so that the total carbonate concentration is 40 mM and the pH 6.2, and the solution was degassed. Stock solutions of each monodentate ligand: imidazole, 2-Me-imidazole, benzimidazole, pyrazole, 4-*t*-buthylphenol, were dissolved in this aqueous buffered solution in separate 5 mL volumetric flasks. The solutions were degassed and an accurately measured volume of a freshly prepared solution of $[V^{IV}O(acac)_2]$ in MeOH (ca. ≈76 mM) was added to ensure a final concentration of ≈2.0 mM in each of the four 5 mL volumetric flasks. The MeOH % was kept constant at 2.7% in the final 5.0 mL solutions. The ligands, except the 4-*tert*-butylphenol, were dissolved in the aqueous buffer medium as stock solutions. Again the proper volume of buffer was added to the 5 mL volumetric flask in order to obtain ratios L:$[V^{IV}O(acac)_2]$ of 0:1, 1:1, 2.5:1 and 5:1. The 4-*tert*-butylphenol (not adequately soluble in water) stock solution was prepared in MeOH; the amounts of $[V^{IV}O(acac)_2]$ and solutions of ligands were then controlled in order to keep the % of organic solvent below 5% and a constant concentration of metal complex of 2.0 mM. The ratios of L:$[V^{IV}O(acac)_2]$ were 0:1, 1:1, 2:1 and 4:1. The two last ratios (with larger amount of the ligands) lead to some precipitation inside of the container. The initial pH of the $[V^{IV}O(acac)_2]$ solution was 7.0±0.2. Upon addition of the ligands the pH values decreased 0.3–0.4 pH units on going from 0:1 to the 4:1 ratios. The absorption spectrum of each of these solutions was measured in the range 380–900 nm, the measurement starting always after the same period of time upon preparing each solu-

tion. Samples were also similarly prepared with lactic acid, but no buffer was added and the pH was adjusted to 6.0 with solutions of HCl or NaOH. Both visible absorption and CD spectra were recorded (section SI-8.4).

Additional details of preparation of solutions are given in the SI section.

4.5.2. Mass and EPR spectra of solutions of $[V^{IV}O(acac)_2]$ and monodentate ligands

A stock solution of $[V^{IV}O(acac)_2]$ (80 mM) was prepared in methanol (previously degassed with N_2). Stock solutions of several monodentate ligands (imidazole, methylimidazole, benzimidazole, pyrazole and phenol) were prepared in 10 mM NH_4CH_3COO aqueous solution (previously set to pH 6.5). All these solutions were degassed with N_2. Accurately measured volumes of each solution of monodentate ligand and of the NH_4CH_3COO aqueous solution were added to six distinct vials using micropipettes, and an accurately measured volume of $[V^{IV}O(acac)_2]$ in methanol was added to each of the six flasks. After the addition of $[V^{IV}O(acac)_2]$ the solutions were purged with a gentle flow of N_2 gas for about 1 minute. Final solutions are 1.1 mM in $[V^{IV}O(acac)_2]$ and ≈2% v/v MeOH. The molar ratio $V^{IV}O$:ligand is 1:7 in all samples and pH values range from 6.58 to 7.15. Additional details are given in the SI section.

For each of the six solutions, ESI-MS (+/-) was carried out ca. 5 minutes after the addition of $[V^{IV}O(acac)_2]$. Samples of these solutions were also introduced in tubes (for EPR spectroscopic measurements) and immediately frozen in liquid N_2.

4.6. Maldi-TOF spectrometric measurements

Sample preparation. $[V^{IV}O(acac)_2]$ stock solutions were prepared in MeOH with ca. 3 mM immediately before mixing. Solutions of apoHTF from PROSPEC were prepared with ca. 300 μM by dissolving the protein in NH_4HCO_3 buffer (pH 7.4, 25 mM). These solutions were allowed to stand overnight to allow equilibration.

Samples for MALDI-TOF MS were prepared with $[V^{IV}O(acac)_2]$:apoHTF molar ratios of 0:1, 1.1, 1:2, 3:1 and 5:1 by mixing different volumes of the stock solutions with buffer. The % of organic solvent was <8% (v/v) and the apoHTF final concentration was either 50 μM (two sets of experiments, or 100 μM (one set with = 0:1, 1.1, 2:1 and 3:1 $[V^{IV}O(acac)_2]$:apoHTF molar ratios). The dried Droplet preparation procedure was used:

Dried Droplet preparation. 2 μL of each sample was mixed with 2 μL of matrix solution (saturated solution of sinapinic acid in 1 mL of 30% (v/v) acetonitrile and 0.1% (v/v) aqueous trifluoroacetic acid). Then 1 μL of the sample-matrix solution was deposited by duplicate onto a MTP 384 ground steel BC target and allowed to dry at room temperature. The apoHTF concentration of the final samples was thus 25 μM.

In one set of experiments two spots were deposited, very close to each other but without contact (at less than ca. 0.5 mm): one containing the apoHTF, the other containing a solution of $[V^{IV}O(acac)_2]$ (see also the SI section). The laser shots were done in a zigzag fashion so that both spots were included. In this way it was possible to check if the formation of $[V^{IV}O(acac)_2]$:apoHTF species could be formed in the gas phase, thus giving false positives. The *m/z* peaks obtained in these experiments were equal to those of apoHTF alone, therefore the existence of false positives can be ruled out (or at least the probability of their existence extremely low).

4.7. Human cells studies; intracellular distribution of $[V^{IV}O(acac)_2]$.

The intracellular distribution of $[V^{IV}O(acac)_2]$ was evaluated in the human A2780 ovarian cancer cells. For the assays cells (~1×10^6/5 mL medium) were cultured in RPMI supplemented with 10% fetal bovine serum (FBS) and exposed to the complex for 24 h (37 °C, 5% CO_2 and humidified atmosphere) at a concentration equivalent to the IC_{50}. The IC_{50} was obtained from a dose-response curve using the MTT cytotoxicity assay. The culture conditions and procedures were similar to previously described methods.[132] After incubation cells were washed with PBS and centrifuged to obtain a pellet; the subcellular soluble protein fractions i.e., cytosol (proteins from cytoplasm), membrane/particulate (membrane proteins including organelles), nuclear fraction (nuclear proteins, including the nuclear membrane proteins) and the cytoskeletal fraction (insoluble proteins and genomic DNA) were extracted using a cell fractionation kit FractionPREP™ (BioVision) following the manufacturer's recommended procedures.

Each cellular fraction was digested with 0.5 mL of distilled conc. HNO_3 in a closed pressurized microwave digestion unit (Mars5, CEM) for 12 h at 150 °C in HP500 vessels and then diluted in ultrapure water to obtain a 2.0% (v/v) acid solution. The vanadium content was measured using a Thermo XSERIES quadrupole ICP-MS instrument (Thermo Scientific). The instrument was calibrated using a multi-element ICP-MS 71 C standard solution (Inorganic Venture). Indium-115 (10 $\mu g\,L^{-1}$) was used as the internal standard.

4.8. DFT calculations.

The full geometry optimization of the molecular structures was carried out at the DFT level of theory using B3P86 functional[133,134] with the help of the Gaussian 09 program package.[135] This functional was found to be appropriate for the theoretical studies of structural parameters and ^{51}V NMR chemical shifts of various V complexes.[92,93,136] The optimization was carried out taking into account solvent effects using the IEFPCM solvation model[137,138] with the UAKS molecular cavity and dispersion, repulsion and cavitation contributions. Water or methanol was used as solvent. No symmetry operations were applied for any of the structures calculated. The geometry optimization was carried out using a relativistic Stuttgart pseudopotential which describes 10 core electrons and the appropriate contracted basis set (8s7p6d1f)/[6s5p3d1f] for the vanadium atom[139] and the 6-31G* basis set for other atoms. The Hessian matrix was calculated analytically for all optimized structures to prove the location of correct minima (no imaginary frequencies) and to estimate the thermodynamic parameters, the latter being calculated at 25 °C.

The single point calculations at the IEFPCM-B3P86/6-311+G** V(ECP)//6-31G* V(ECP) level of theory were then carried out. The basis set corrected enthalpies and Gibbs free energies in solution (H_s and G_s) discussed in the text, were calculated using the following equations:

$$H_s = E_s(\text{6-311+G**}) - E_s(\text{6-31G*}) + H_s(\text{6-31G*}) \quad (5)$$

$$G_s = E_s(\text{6-311+G**}) - E_s(\text{6-31G*}) + G_s(\text{6-31G*}) \quad (6)$$

The ^{51}V hyperfine coupling constants were estimated in gas phase at the single-point calculations using the BHandHLYP functional and 6–311+G** basis set for all atoms on the basis of the equilibrium geometry obtained at the IEFPCM-B3P86/6-31G*(V-ECP) level of theory. The anisotropic ^{51}V hyperfine coupling constants A_x, A_y and A_z were estimated as the sum of the isotropic Fermi contact

term and corresponding dipolar hyperfine interaction term.[140] Wave functions were verified for their stability using the keyword STABLE in Gaussian. If necessary, they were reoptimized to achieve a stable solution.

Acknowledgements

We thank L. Fernandes for assistance preparing the samples for Maldi-TOF analysis. This work was supported by Fundação *para* a Ciência e Tecnologia (FCT), Portugal (projects UID/Multi/04349/2013, UID/QUI/00100/2013, RECI/QEQ-QIN/0189/2012, RECI/QEQMED/0330/2012, PTDC/QEQ-MED/1902/2014 and doctoral grant SFRH/BD/77894/2011 to M.F.A.S) and programme FCT Investigator: IF/00100/2013 (IC) and IF/00007/2015 (H.M.S.). The PROTEOMASS Scientific Society is acknowledged by the funding provided to the Biological Mass Spectrometry *Isabel Moura*. H.M.S., J.L.C., M.F.A.S. and T.S.S acknowledge the funding provided by UCIBIO, Unidade de Ciências Biomoleculares Aplicadas, (UID/Multi/04378/2013) and co-financed by the ERDF under the PT2020 Partnership Agreement (POCI-01-0145-FEDER-007728). H.M.S. and J.L.C. also acknowledge the Associate Laboratory for Green Chemistry LAQV (UID/QUI/50006/2013) and co-financed by the ERDF under the PT2020 Partnership Agreement (POCI-01-0145-FEDER-007265). The Portuguese NMR and Mass Spectrometry IST-UL Centers are also acknowledged for the access to the equipment. The authors would also like to thank the ESRF (Grenoble, France) for providing the access to the SAXS facilities (beamline BM29)."

Conflict of interest

The authors declare no conflict of interest.

Keywords: acetylacetonate · circular dichroism · mass spectrometry · transferrin

[1] R. P. Dodge, A. Zalkin, D. H. Templeton, *J. Chem. Phys.* **1961**, *35*, 55 – 67.
[2] M. W. Makinen, M. Salehitazangi, *Coord. Chem. Rev.* **2014**, *279*, 1 – 22.
[3] L. F. Vilas Boas, J. Costa Pessoa in *Comprehensive Coordination Chemistry, Vol. 3* (Eds.: G. Wilkinson, R. D. Gillard, J. A. McCleverty), Pergamon Press, Oxford, **1987**, pp. 453 – 583.
[4] D. C. Crans, A. R. Khan, M. Mahroof-Tahir, S. Mondal, S. M. Miller, A. la Cour, O. P. Anderson, T. Jakusch, T. Kiss, *J. Chem. Soc. Dalton Trans.* **2001**, 3337 – 3345.
[5] M. R. Maurya, B. Uprety, F. Avecilla, P. Adão, J. C. Pessoa, *Dalton Trans.* **2015**, *44*, 17736 – 17755.
[6] M. R. Maurya, N. Chaudhary, F. Avecilla, P. Adão, J. C. Pessoa, *Dalton Trans.* **2015**, *44*, 1211 – 1232.
[7] M. R. Maurya, *Coord. Chem. Rev.* **2003**, *237*, 163 – 181.
[8] G. Scalese, J. Benitez, S. Rostan, I. Correia, L. Bradford, M. Vieites, L. Minini, A. Merlino, E. L. Coitino, E. Birriel, J. Varela, H. Cerecetto, M. Gonzalez, J. C. Pessoa, D. Gambino, *J. Inorg. Biochem.* **2015**, *147*, 116 – 125.
[9] M. Fernez, J. Varela, I. Correia, E. Birriel, J. Castiglioni, V. Moreno, J. C. Pessoa, H. Cerecetto, M. Gonzalez, D. Gambino, *Dalton Trans.* **2013**, *42*, 11900 – 11911.
[10] M. Kirihara, *Coord. Chem. Rev.* **2011**, *255*, 2281 – 2302.
[11] D. R. Hwang, C. P. Chen, B. J. Uang, *Chem. Commun.* **1999**, 1207 – 1208.
[12] H. B. Liu, M. Wang, Y. Wang, Y. Wang, H. Sun, L. C. Sun, *Catal. Commun.* **2009**, *11*, 294 – 297.
[13] T. Hirao, *Chem. Rev.* **1997**, *97*, 2707 – 2724.
[14] T. Itoh, K. Jitsukawa, K. Kaneda, S. Teranishi, *J. Am. Chem. Soc.* **1979**, *101*, 159 – 169.
[15] C. Pereira, J. F. Silva, A. M. Pereira, J. P. Araujo, G. Blanco, J. M. Pintado, C. Freire, *Catal. Sci. Technol.* **2011**, *1*, 784 – 793.
[16] M. Z. Mehdi, A. K. Srivastava, *Arch. Biochem. Biophys.* **2005**, *440*, 158 – 164.
[17] S. S. Amin, K. Cryer, B. Y. Zhang, S. K. Dutta, S. S. Eaton, O. Person, S. M. Miller, B. A. Reul, S. M. Brichard, D. C. Crans, *Inorg. Chem.* **2000**, *39*, 406 – 416.
[18] B. A. Reul, S. S. Amin, J. P. Buchet, L. N. Ongemba, D. C. Crans, S. M. Brichard, *Br. J. Pharmacol.* **1999**, *126*, 467 – 477.
[19] J. X. Wu, Y. H. Hong, X. G. Yang, *J. Biol. Inorg. Chem.* **2016**, *21*, 919 – 929.
[20] N. Butenko, J. P. Pinheiro, J. P. da Silva, A. I. Tomaz, I. Correia, V. Ribeiro, J. C. Pessoa, I. Cavaco, *J. Inorg. Biochem.* **2015**, *147*, 165 – 176.
[21] N. Butenko, A. I. Tomaz, O. Nouri, E. Escribano, V. Moreno, S. Gama, V. Ribeiro, J. P. Telo, J. C. Pessoa, I. Cavaco, *J. Inorg. Biochem.* **2009**, *103*, 622 – 632.
[22] X. G. Yang, X. D. Yang, L. Yuan, K. Wang, D. C. Crans, *Pharm. Res.* **2004**, *21*, 1026 – 1033.
[23] Y. Fu, Q. Wang, X. G. Yang, X. D. Yang, K. Wang, *J. Biol. Inorg. Chem.* **2008**, *13*, 1001 – 1009.
[24] J. C. Pessoa, S. Etcheverry, D. Gambino, *Coord. Chem. Rev.* **2015**, *301*, 24 – 48.
[25] J. Costa Pessoa, *J. Inorg. Biochem.* **2015**, *147*, 4 – 24.
[26] S. Mehtab, G. Goncalves, S. Roy, A. I. Tomaz, T. Santos-Silva, M. F. A. Santos, M. J. Romao, T. Jakusch, T. Kiss, J. C. Pessoa, *J. Inorg. Biochem.* **2013**, *121*, 187 – 195.
[27] D. Sanna, L. Biro, P. Buglyo, G. Micera, E. Garribba, *Metallomics* **2012**, *4*, 33 – 36.
[28] T. Jakusch, J. C. Pessoa, T. Kiss, *Coord. Chem. Rev.* **2011**, *255*, 2218 – 2226.
[29] D. Sanna, G. Micera, E. Garribba, *Inorg. Chem.* **2010**, *49*, 174 – 187.
[30] J. Costa Pessoa, I. Tomaz, *Curr. Med. Chem.* **2010**, *17*, 3701 – 3738.
[31] T. Jakusch, D. Hollender, E. A. Enyedy, C. S. Gonzalez, M. Montes-Bayon, A. Sanz-Medel, J. C. Pessoa, I. Tomaz, T. Kiss, *Dalton Trans.* **2009**, 2428 – 2437.
[32] T. Kiss, T. Jakusch, D. Hollender, A. Dornyei, E. A. Enyedy, J. C. Pessoa, H. Sakurai, A. Sanz-Medel, *Coord. Chem. Rev.* **2008**, *252*, 1153 – 1162.
[33] A. Levina, A. I. McLeod, S. J. Gasparini, A. Nguyen, W. G. M. Silva, J. B. Aitken, H. H. Harris, C. Glover, B. Johannessen, P. A. Lay, *Inorg. Chem.* **2015**, *54*, 7753 – 7766.
[34] D. Sanna, M. Serra, G. Micera, E. Garribba, *Inorg. Chem.* **2014**, *53*, 1449 – 1464.
[35] G. R. Willsky, K. Halvorsen, M. E. Godzala, L. H. Chi, M. J. Most, P. Kaszynski, D. C. Crans, A. B. Goldfine, P. J. Kostyniak, *Metallomics* **2013**, *5*, 1491 – 1502.
[36] K. H. Thompson, J. Lichter, C. Lebel, M. C. Scaife, J. H. McNeill, C. Orvig, *J. Inorg. Biochem.* **2009**, *103*, 554 – 558.
[37] J. Costa Pessoa, G. Goncalves, S. Roy, I. Correia, S. Mehtab, M. F. A. Santos, T. Santos-Silva, *Inorg. Chim. Acta* **2014**, *420*, 60 – 68.
[38] M. W. Makinen, M. J. Brady, *J. Biol. Chem.* **2002**, *277*, 12215 – 12220.
[39] D. Mustafi, B. Peng, S. Foxley, M. W. Makinen, G. S. Karczmar, M. Zamora, J. Ejnik, H. Martin, *J. Biol. Inorg. Chem.* **2009**, *14*, 1187 – 1197.
[40] H. S. Ou, L. M. Yan, D. Mustafi, M. W. Makinen, M. J. Brady, *J. Biol. Inorg. Chem.* **2005**, *10*, 874 – 886.
[41] P. Holko, J. Ligeza, J. Kisielewska, A. M. Kordowiak, A. Klein, *Polish J. Pathol.* **2008**, *59*, 3 – 8.
[42] M. W. Makinen, R. Bamba, L. Ikejimba, C. Wietholt, C. T. Chen, S. D. Conzen, *Dalton Trans.* **2013**, *42*, 11862 – 11867.
[43] D. Sanna, G. Micera, E. Garribba, *Inorg. Chem.* **2011**, *50*, 3717 – 3728.
[44] D. Sanna, P. Buglyo, G. Micera, E. Garribba, *J. Biol. Inorg. Chem.* **2010**, *15*, 825 – 839.
[45] D. Sanna, G. Micera, E. Garribba, *Inorg. Chem.* **2013**, *52*, 11975 – 11985.
[46] J. Selbin, *Chem. Rev.* **1965**, *65*, 153 – 175.
[47] R. L. Carlin, F. A. Walker, *J. Am. Chem. Soc.* **1965**, *87*, 2128 – 2133.
[48] E. Kwiatkowski, J. Trojanowski, *J. Inorg. Nucl. Chem.* **1976**, *38*, 131 – 135.
[49] E. Garribba, G. Micera, D. Sanna, *Inorg. Chim. Acta* **2006**, *359*, 4470 – 4476.
[50] K. Isobe, Y. Nakamura, S. Kawaguchi, *J. Inorg. Nucl. Chem.* **1978**, *40*, 607 – 611.
[51] B. Kirste, H. Vanwilligen, *J. Phys. Chem.* **1982**, *86*, 2743 – 2749.

[52] J. J. R. da Silva, R. Wootton, *J. Chem. Soc. D* **1969**, 421b – 422.
[53] B. M. Sawant, A. L. Shroyer, G. R. Eaton, S. S. Eaton, *Inorg. Chem.* **1982**, *21*, 1093 – 1101.
[54] M. R. Caira, J. M. Haigh, L. R. Nassimbeni, *J. Inorg. Nucl. Chem.* **1972**, *34*, 3171 – 3176.
[55] C. M. Guzy, J. B. Raynor, M. C. R. Symons, *J. Chem. Soc. Inorg. Phys. Theor.* **1969**, 2791 – 2795.
[56] N. D. Yordanov, M. Zdravkova, *Polyhedron* **1993**, *12*, 635 – 639.
[57] N. M. Atherton, P. J. Gibbon, M. C. B. Shohoji, *J. Chem. Soc. Dalton Trans.* **1982**, 2289 – 2290.
[58] D. Mustafi, M. W. Makinen, *Inorg. Chem.* **2005**, *44*, 5580 – 5590.
[59] M. R. Caira, L. R. Nassimbeni, J. M. Haigh, *Inorg. Nucl. Chem. Lett.* **1972**, *8*, 109 – 112.
[60] M. C. Shao, L. F. Wang, Z. Y. Zhang, *Acta Chim. Sin.* **1983**, *41*, 985 – 992.
[61] K. Dichmann, G. Hamer, S. C. Nyburg, W. F. Reynolds, *J. Chem. Soc. Chem. Commun.* **1970**, 1295 – 1296.
[62] T. Kolesa-Dobravc, A. Meden, F. Perdih, *Acta Chim. Slov.* **2015**, *62*, 261 – 271.
[63] T. F. S. Silva, T. C. O. Mac Leod, L. M. D. R. S. Martins, M. F. C. G. da Silva, M. A. Schiavon, A. J. L. Pombeiro, *J. Mol. Catal. A* **2013**, *367*, 52 – 60.
[64] R. T. A. Macgillivray, E. Mendez, S. K. Sinha, M. R. Sutton, J. Linebackzins, K. Brew, *Proc. Natl. Acad. Sci. USA* **1982**, *79*, 2504 – 2508.
[65] D. C. Crans, *J. Inorg. Biochem.* **2000**, *80*, 123 – 131.
[66] M. Helena, S. F. Teixeira, J. C. Pessoa, L. F. V. Boas, *Polyhedron* **1992**, *11*, 697 – 708.
[67] J. C. Pessoa, I. Tomaz, T. Kiss, E. Kiss, P. Buglyo, *J. Biol. Inorg. Chem.* **2002**, *7*, 225 – 240.
[68] J. C. Pessoa, L. F. V. Boas, R. D. Gillard, R. J. Lancashire, *Polyhedron* **1988**, *7*, 1245 – 1262.
[69] J. C. Pessoa, I. Tomaz, T. Kiss, P. Buglyo, *J. Inorg. Biochem.* **2001**, *84*, 259 – 270.
[70] J. C. Pessoa, T. Gajda, R. D. Gillard, T. Kiss, S. M. Luz, J. J. G. Moura, I. Tomaz, J. P. Telo, I. Torok, *J. Chem. Soc. Dalton Trans.* **1998**, 3587 – 3600.
[71] J. C. Pessoa, R. L. Marques, L. F. V. Boas, R. D. Gillard, *Polyhedron* **1990**, *9*, 81 – 98.
[72] J. C. Pessoa, S. M. Luz, R. D. Gillard, *J. Chem. Soc. Dalton Trans.* **1997**, 569 – 576.
[73] T. Kiss, T. Jakusch, J. C. Pessoa, I. Tomaz, *Coord. Chem. Rev.* **2003**, *237*, 123 – 133.
[74] V. B. Di Marco, G. G. Bombi, *Mass Spectrom. Rev.* **2006**, *25*, 347 – 379.
[75] E. N. Kitova, A. El-Hawiet, P. D. Schnier, J. S. Klassen, *J. Am. Soc. Mass Spectrom.* **2012**, *23*, 431 – 441.
[76] T. Jakusch, A. Dornyei, I. Correia, L. M. Rodrigues, G. K. Toth, T. Kiss, J. C. Pessoa, S. Marcão, *Eur. J. Inorg. Chem.* **2003**, 2113 – 2122.
[77] J. C. Pessoa, I. Correia, G. Gonçalves, A. I. Tomaz, *J. Argent. Chem. Soc.* **2009**, *97*, 151 – 165.
[78] G. Gonçalves, I. Tomaz, I. Correia, L. F. Veiros, M. M. C. A. Castro, F. Avecilla, L. Palacio, M. Maestro, T. Kiss, T. Jakusch, M. H. V. Garcia, J. C. Pessoa, *Dalton Trans.* **2013**, *42*, 11841 – 11861.
[79] M. F. A. Santos, I. Correia, A. R. Oliveira, E. Garribba, J. C. Pessoa, T. Santos-Silva, *Eur. J. Inorg. Chem.* **2014**, 3293 – 3297.
[80] M. V. Petoukhov, D. Franke, A. V. Shkumatov, G. Tria, A. G. Kikhney, M. Gajda, C. Gorba, H. D. T. Mertens, P. V. Konarev, D. I. Svergun, *J. Appl. Crystallogr.* **2012**, *45*, 342 – 350.
[81] J. Wally, P. J. Halbrooks, C. Vonrhein, M. A. Rould, S. J. Everse, A. B. Mason, S. K. Buchanan, *J. Biol. Chem.* **2006**, *281*, 24934 – 24944.
[82] D. Svergun, C. Barberato, M. H. J. Koch, *J. Appl. Crystallogr.* **1995**, *28*, 768 – 773.
[83] T. J. F. Hillenkamp, M. Karas, *MALDI MS—A Practical Guide to Instrumentation, Methods Applications* (Ed.: F. Hillenkamp, J. Peter-Katalinic), Wiley-VCH, Weinheim, **2007**, pp. 16 – 18.
[84] N. D. Chasteen in *Vanadyl(IV) EPR spin probe. Inorganic Biochemical Aspects, Vol. 3* (Eds.: L. J. J. Berliner, J. Reuben), Plenum Press, New York, **1981**, pp. 53 – 119.
[85] T. S. Smith, R. LoBrutto, V. L. Pecoraro, *Coord. Chem. Rev.* **2002**, *228*, 1 – 18.
[86] T. S. Smith, C. A. Root, J. W. Kampf, P. G. Rasmussen, V. L. Pecoraro, *J. Am. Chem. Soc.* **2000**, *122*, 767 – 775.
[87] M. R. Maurya, J. C. Pessoa, *J. Organomet. Chem.* **2011**, *696*, 244 – 254.
[88] B. D. Liboiron, K. H. Thompson, G. R. Hanson, E. Lam, N. Aebischer, C. Orvig, *J. Am. Chem. Soc.* **2005**, *127*, 5104 – 5115.
[89] D. Sanna, E. Garribba, G. Micera, *J. Inorg. Biochem.* **2009**, *103*, 648 – 655.
[90] A. Rockenbauer, L. Korecz, *Appl. Magn. Reson.* **1996**, *10*, 29 – 43.
[91] T. Jakusch, A. Dean, T. Oncsik, A. C. Benyei, V. Di Marco, T. Kiss, *Dalton Trans.* **2010**, *39*, 212 – 220.
[92] M. R. Maurya, A. Arya, A. Kumar, M. L. Kuznetsov, F. Avecilla, J. C. Pessoa, *Inorg. Chem.* **2010**, *49*, 6586 – 6600.
[93] M. R. Maurya, M. Bisht, A. Kumar, M. L. Kuznetsov, F. Avecilla, J. C. Pessoa, *Dalton Trans.* **2011**, *40*, 6968 – 6983.
[94] M. R. Maurya, A. Arya, A. Kumar, J. C. Pessoa, *Dalton Trans.* **2009**, 2185 – 2195.
[95] C. Pereira, A. R. Silva, A. P. Carvalho, J. Pires, C. Freire, *J. Mol. Catal. A* **2008**, *283*, 5 – 14.
[96] M. Baltes, O. Collart, P. Van der Voort, E. F. Vansant, *Langmuir* **1999**, *15*, 5841 – 5845.
[97] A. Lattanzi, N. E. Leadbeater, *Org. Lett.* **2002**, *4*, 1519 – 1521.
[98] J. J. P. Stewart, *J. Mol. Model.* **2013**, *19*, 1 – 32.
[99] J. J. P. Stewart, MOPAC2016, Stewart Computational Chemistry, Colorado Springs, CO, USA, http://OpenMOPAC.net, **2016**.
[100] G. Micera, E. Garribba, *Int. J. Quantum Chem.* **2012**, *112*, 2486 – 2498.
[101] R. T. A. MacGillivray, S. A. Moore, J. Chen, B. F. erson, H. Baker, Y. G. Luo, M. Bewley, C. A. Smith, M. E. P. Murphy, Y. Wang, A. B. Mason, R. C. Woodworth, G. D. Brayer, E. N. Baker, *Biochemistry* **1998**, *37*, 7919 – 7928.
[102] P. J. Halbrooks, A. B. Mason, T. E. Adams, S. K. Briggs, S. J. Everse, *J. Mol. Biol.* **2004**, *339*, 217 – 226.
[103] P. D. Jeffrey, M. C. Bewley, R. T. A. MacGillivray, A. B. Mason, R. C. Woodworth, E. N. Baker, *Biochemistry* **1998**, *37*, 13978 – 13986.
[104] G. C. Justino, E. Garribba, J. C. Pessoa, *J. Biol. Inorg. Chem.* **2013**, *18*, 803 – 813.
[105] J. Honzicek, J. Vinklarek, *Inorg. Chim. Acta* **2015**, *437*, 87 – 94.
[106] P. Ghosh, S. Ghosh, C. Navara, R. K. Narla, A. Benyumov, F. M. Uckun, *J. Inorg. Biochem.* **2001**, *84*, 241 – 253.
[107] S. S. Lehrer, *J. Biol. Chem.* **1969**, *244*, 3613 – 3617.
[108] N. G. James, J. A. Ross, A. B. Mason, D. M. Jameson, *Protein Sci.* **2010**, *19*, 99 – 110.
[109] N. G. James, C. L. Berger, S. L. Byrne, V. C. Smith, R. T. A. MacGillivray, A. B. Mason, *Biochemistry* **2007**, *46*, 10603 – 10611.
[110] P. R. Callis, T. Q. Liu, *J. Phys. Chem. B* **2004**, *108*, 4248 – 4259.
[111] H. Y. Du, J. F. Xiang, Y. Z. Zhang, Y. L. Tang, G. Z. Xu, *J. Inorg. Biochem.* **2008**, *102*, 146 – 149.
[112] M. van de Weert, *J. Fluoresc.* **2010**, *20*, 625 – 629.
[113] M. van de Weert, L. Stella, *J. Mol. Struct.* **2011**, *998*, 144 – 150.
[114] W. R. Ware, *J. Phys. Chem.* **1962**, *66*, 455 – 458.
[115] D. Sanna, G. Micera, E. Garribba, *Inorg. Chem.* **2009**, *48*, 5747 – 5757.
[116] I. Correia, T. Jakusch, E. Cobbinna, S. Mehtab, I. Tomaz, N. V. Nagy, A. Rockenbauer, J. C. Pessoa, T. Kiss, *Dalton Trans.* **2012**, *41*, 6477 – 6487.
[117] E. Cobbina, S. Mehtab, I. Correia, G. Goncalves, I. Tomaz, I. Cavaco, T. Jakusch, E. Enyedi, T. Kiss, J. C. Pessoa, *J. Mex. Chem. Soc.* **2013**, *57*, 180 – 191.
[118] W. Bal, J. Christodoulou, P. J. Sadler, A. Tucker, *J. Inorg. Biochem.* **1998**, *70*, 33 – 39.
[119] J. R. Lakowicz, *Principles of Fluorescence Spectroscopy*, Springer, New York, **2006**.
[120] A. Sulkowska, *J. Mol. Struct.* **2002**, *614*, 227 – 232.
[121] G. Scalese, I. Correia, J. Benitez, S. Rostan, F. Marques, F. Mendes, A. P. Matos, J. C. Pessoa, D. Gambino, *J. Inorg. Biochem.* **2017**, *166*, 162 – 172.
[122] M. H. Nagaoka, H. Akiyama, T. Maitani, *Analyst* **2004**, *129*, 51 – 54.
[123] K. G. Fernes, M. Montes-Bayon, E. B. Gonzalez, E. Del Castillo-Busto, J. A. Nobrega, A. Sanz-Medel, *J. Anal. At. Spectrom.* **2005**, *20*, 210 – 215.
[124] A. Levina, A. I. McLeod, L. E. Kremer, J. B. Aitken, C. J. Glover, B. Johannessen, P. A. Lay, *Metallomics* **2014**, *6*, 1880 – 1888.
[125] N. D. Chasteen, *Coord. Chem. Rev.* **1977**, *22*, 1 – 36.
[126] N. D. Chasteen, J. K. Grady, C. E. Holloway, *Inorg. Chem.* **1986**, *25*, 2754 – 2760.
[127] K. Hirayama, S. Akashi, M. Furuya, K. Fukuhara, *Biochem. Biophys. Res. Commun.* **1990**, *173*, 639 – 646.
[128] P. Pernot, A. Round, R. Barrett, A. D. Antolinos, A. Gobbo, E. Gordon, J. Huet, J. Kieffer, M. Lentini, M. Mattenet, C. Morawe, C. Mueller-Dieckmann, S. Ohlsson, W. Schmid, J. Surr, P. Theveneau, L. Zerrad, S. McSweeney, *J. Synchrotron Radiat.* **2013**, *20*, 660 – 664.

[129] A. Round, F. Felisaz, L. Fodinger, A. Gobbo, J. Huet, C. Villard, C. E. Blanchet, P. Pernot, S. McSweeney, M. Roessle, D. I. Svergun, F. Cipriani, *Acta Crystallogr. Sect. D* **2015**, *71*, 67 – 75.
[130] D. Franke, D. I. Svergun, *J. Appl. Crystallogr.* **2009**, *42*, 342 – 346.
[131] V. V. Volkov, D. I. Svergun, *J. Appl. Crystallogr.* **2003**, *36*, 860 – 864.
[132] I. Correia, S. Roy, C. P. Matos, S. Borovic, N. Butenko, I. Cavaco, F. Marques, J. Lorenzo, A. Rodriguez, V. Moreno, J. C. Pessoa, *J. Inorg. Biochem.* **2015**, *147*, 134 – 146.
[133] A. D. Becke, *J. Chem. Phys.* **1993**, *98*, 5648 – 5652.
[134] J. P. Perdew, *Phys. Rev. B* **1986**, *33*, 8822 – 8824.
[135] Gaussian 09, revision C.01, M. J. Frisch, G. W. Trucks, H. B. Schlegel, G. E. Scuseria, M. A. Robb, J. R. Cheeseman, G. Scalmani, V. Barone, B. Mennucci, G. A. Petersson, H. Nakatsuji, M. Caricato, X. Li, H. P. Hratchian, A. F. Izmaylov, J. Bloino, G. Zheng, J. L. Sonnenberg, M. Hada, M. Ehara, K. Toyota, R. Fukuda, J. Hasegawa, M. Ishida, T. Nakajima, Y. Honda, O. Kitao, H. Nakai, T. Vreven, J. A. Montgomery, Jr., J. E. Peralta, F. Ogliaro, M. Bearpark, J. J. Heyd, E. Brothers, K. N. Kudin, V. N. Staroverov, T. Keith, R. Kobayashi, J. Norm, K. Raghavachari, A. Rendell, J. C. Burant, S. S. Iyengar, J. Tomasi, M. Cossi, N. Rega, J. M. Millam, M. Klene, J. E. Knox, J. B. Cross, V. Bakken, C. Adamo, J. Jaramillo, R. Gomperts, R. E. Stratmann, O. Yazyev, A. J. Austin, R. Cammi, C. Pomelli, J. W. Ochterski, R. L. Martin, K. Morokuma, V. G. Zakrzewski, G. A. Voth, P. Salvador, J. J. Dannenberg, S. Dapprich, A. D. Daniels, Ö. Farkas, J. B. Foresman, J. V. Ortiz, J. Cioslowski, D. J. Fox, Gaussian, Inc., Wallingford, CT, **2010**.
[136] M. R. Maurya, C. Haldar, A. Kumar, M. L. Kuznetsov, F. Avecilla, J. C. Pessoa, *Dalton Trans.* **2013**, *42*, 11941 – 11962.
[137] V. Barone, M. Cossi, *J. Phys. Chem. A* **1998**, *102*, 1995 – 2001.
[138] G. Scalmani, M. J. Frisch, *J. Chem. Phys.* **2010**, *132*, 114110.
[139] M. Dolg, U. Wedig, H. Stoll, H. Preuss, *J. Chem. Phys.* **1987**, *86*, 866 – 872.
[140] S. Gorelsky, G. Micera, E. Garribba, *Chem. Eur. J.* **2010**, *16*, 8167 – 8180.

Manuscript received: March 28, 2017
Revised manuscript received: May 29, 2017
Accepted manuscript online: June 26, 2017
Version of record online: July 20, 2017